Assemblies of lauryl maltose neopentyl glycol (LMNG) and LMNG-solubilized membrane proteins

Cécile Breyton, Waqas Javed, Anne Vermot, Charles-Adrien Arnaud, Christine Hajjar, Jérôme Dupuy, Isabelle Petit-Härtlein, Aline Le Roy, Anne Martel, Michel Thépaut, et al.

Assemblies of lauryl maltose neopentyl glycol (LMNG) and LMNG-solubilized membrane proteins

Cécile Breyton[1], Waqas Javed[1,2], Annelise Vermot[1], Charles-Adrien Arnaud[1], Christine Hajjar[1], Jérôme Dupuy[1], Isabelle Petit-Hartlein[1], Aline Le Roy[1], Anne Martel[3], Michel Thépaut[1], Cédric Orelle[2], Jean-Michel Jault[2], Franck Fieschi[1], Lionel Porcar[3], Christine Ebel[1*]

[1] Univ. Grenoble Alpes, CNRS, CEA, Institute for Structural Biology (IBS), 38000 Grenoble, France
[2] University of Lyon, CNRS, UMR5086, Molecular Microbiology and Structural Biochemistry, IBCP, Lyon 69367 France.
[3] Institut Max Von Laue Paul Langevin, 38042 Grenoble, France

*Corresponding author.

Keywords
Membrane proteins – Detergent – LMNG – homogeneity – crystallization – rods

Footnotes
AUC: Analytical Ultracentrifugation ; DSF: Differential Scanning Fluorimetry; SEC-LS: Size Exclusion Chromatography coupled to Light Scattering; SAXS: Small Angle X-Ray Scattering; SANS: Small Angle Neutron Scattering; TLC: Thin Layer Chromatography; CMC: critical micelle concentration ; DDM: dodecyl-β-D-maltopyranoside; DDAO: decyldimethylamine-N-oxide; LDAO: lauryldimethylamine-N-oxide; LMNG: lauryl maltose neopentyl glycol; OTG: octyl-β-D-thioglucopyranoside; bR: bacteriorhodopsin from *Halobacterium*; BmrA: Bacillus multidrug resistance ATP; SpNOX: *S. pneumoniae* NOX protein; FhuA: *E. coli* outer membrane ferrichome-iron transporter. Vi: orthovanadate;

Abstract

Laurylmaltose neopentylglycol (LMNG) bears two linked hydrophobic chains of equal length and two hydrophilic maltoside groups. It arouses a strong interest in the field of membrane protein biochemistry, since it was shown to efficiently solubilize and stabilize membrane proteins often better than the commonly used dodecylmaltopyranoside (DDM), and to allow structure determination of some challenging membrane proteins. However, LMNG was described to form large micelles, which could be unfavorable for structural purposes. We thus investigated its auto-assemblies and the association state of different membrane proteins solubilized in LMNG by analytical ultracentrifugation, size exclusion chromatography coupled to light scattering, centrifugation on sucrose gradient and/or small angle scattering. At high concentrations (in the mM range) LMNG forms long rods, and it stabilized the membrane proteins investigated herein, *i.e*. a bacterial multidrug transporter, BmrA; a prokaryotic analogous of the eukaryotic NADPH oxidases, SpNOX; an *E. coli* outer membrane transporter, FhuA; and the halobacterial bacteriorhodopsin, bR. BmrA, in the Apo and the vanadate-inhibited forms showed reduced kinetics of limited proteolysis in LMNG compared to DDM. Both SpNOX and BmrA display an increased specific activity in LMNG compared to DDM. The four proteins form LMNG complexes with their usual quaternary structure and with usual amount of bound detergent. No heterogeneous complexes related to the large micelle size of LMNG alone were observed. In conditions where LMNG form assemblies of large size, FhuA crystals diffracting to 4.0 Å were obtained by vapor diffusion. LMNG large micelle size thus does not preclude membrane protein homogeneity and crystallization.

Introduction

Detergents are amphipatic molecules that auto-assemble into micelles above the critical micelle concentration (CMC). Above the CMC, they are able to solubilize lipids and membrane proteins, forming protein-detergent complexes of small and well-defined size [1]. Detergents are essential for membrane protein solubilization and purification steps, as well as functional and structural studies. However, they often lead to membrane protein inactivation. One of the mechanisms leading to inactivation (for a recent review, see [2]) is the dissociation of subunits, loss of essential lipids or other hydrophobic co-factors. As an example, cytochrome b_6f inactivation and monomerization was related to lipid loss [3]. Detergent dynamics, *i.e.* detergent exchange between the free monomers, or between micelles, and bound detergent at the surface of the transmembrane protein surface, could trigger transient exposure of this hydrophobic surface leading to irreversible protein aggregation. Detergent binding can also alter protein structure: molecular dynamics simulation indeed showed, for a thermostable mutant of the adenosine receptor, that the harsh octylglucoside detergent molecules intercalate between trans-membrane helices, moving them apart in the 200 ns simulation [4]. The structure and dynamics of different α-helical membrane proteins solubilized in alkyl phosphocholines appear deeply altered [5]. For example, NMR, molecular dynamics simulations, and functional studies, amongst other techniques, show that mitochondrial carriers are incorrectly folded in these detergents. Some parts of the transmembrane segments are disordered, with molecules of detergent penetrating between the helices; the proteins are in a highly dynamic state with unstable tertiary contacts; and weak ligand binding results from non-specific interactions [5]. In the challenging aim to obtain high resolution structure of membrane proteins by crystallography, a usual strategy is to select

detergents that not only preserve membrane protein stability, function and solubility, but also form small micelles (*e.g.* by adding compounds decreasing the micelle size), in order to favor protein-protein contacts [6,7].

The propensity of detergents to inactivate membrane proteins drove the search for new amphiphilic environnements (for a review, see [6,8,9]). Peptides that form an α-helix or a β-sheet [10–13], amphipatic polymers with multiple hydrophobic tails [14,15], fluorinated surfactants (reviewed in [8,16,17]), Calixarene based detergents (*e.g.* [18]) or detergents with varying architectures: tripod amphiphiles (*e.g.* [19,20]), facial amphiphiles [21–23], polycyclic based [24], bi-tails [25–29], tri-tails [30], and other compounds [31–33] have been synthetized to decrease their exchange kinetics, and/or reinforce interactions with membrane protein surfaces. This is done noticeably by increasing the rigidity as well as the surface of their hydrophobic moieties. Among these compounds, neopentyl glycols (MNG) constitute a class of detergents with notable interest [25,26]. Members with different chain lengths or with different sugar head groups have been described and are commercialized (Anatrace). We will focus here on the most commonly used one, lauryl maltose neopentyl glycol (LMNG), also named MNG3 (MNG3, however, designates the related family of compounds in [26]). Its structure (Scheme 1) is formed by two molecules of n-dodecyl-β-D-maltopyranoside (DDM) linked at the junction between the hydrophilic and hydrophobic moieties of the molecule. The presence of the two hydrophobic chains of equal length mimics better the structure of lipids than classical detergents having a single hydrophobic tail. According to the authors who designed this detergent in 2010, the central quaternary carbon, was "intended to place subtle restraints on conformational flexibility" [26]. In this work, LMNG was shown to display a set of very interesting features: to extract integral membrane proteins from membranes; to improve substantially the stability of various membrane proteins, including G protein-coupled receptors and respiratory complexes. It also allowed diffraction up to 3.4 Å resolution of LMNG-solubilized cytochrome b_6f crystals obtained by vapor diffusion [26]. Shortly after this first publication, high resolution structures of the challenging β2 adrenergic receptor, in complex with G-proteins [34] or with covalently bound agonist [35], were obtained. The proteins were solubilized and purified in LMNG followed by crystallization in mesophase. LMNG was then described as successfully used for various applications, including membrane solubilization and membrane protein stabilization (*e.g.* [26,36–40]), excited state intermediates [37,41–44], NMR studies [44], H/D exchange coupled to mass spectroscopy (*e.g.* [45,46]), negative stain electron microscopy (*e.g.* [43,46,47]), or reconstitution in lipid vesicles [48]. Impressively, LMNG has now been used to solve the structure of more than ten G-protein coupled receptors (*e.g.* refs in [49]; in all cases, LMNG was used for protein purification and crystallization was performed in mesophase). Other proteins, *e.g.* ABC transporters [41,50,51] or channels [52], were purified and cystallized in LMNG by vapor diffusion. Furthermore, LMNG was also successfully used to solve the high resolution structures of membrane proteins by single particle cryo-electron microscopy (*e.g.* [47,53–55]).

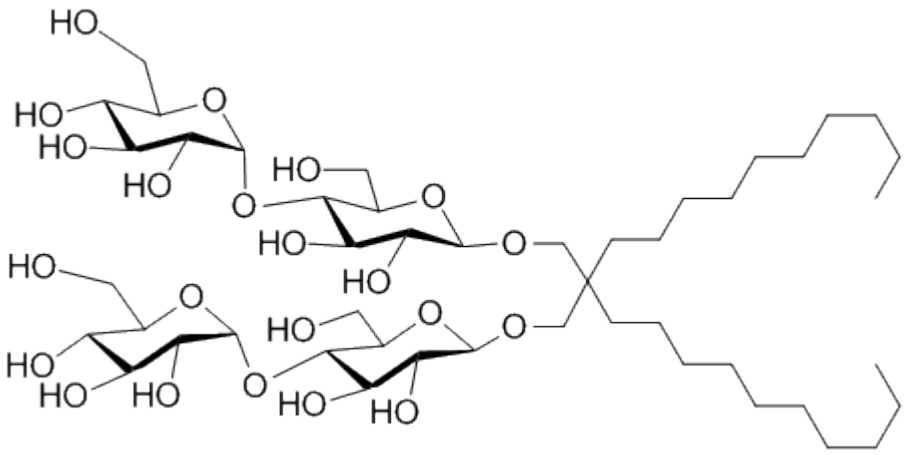

Scheme 1: Chemical structure of LMNG

Regarding the β2 adrenergic receptor in complex with G-proteins, not only does the complex display long term stabilization in LMNG, but surprisingly, its ligand binding activity is preserved even after diluting LMNG 1000 fold below its CMC [34]. The kinetics of interconversion between the different β2 adrenergic receptor conformations are significantly slower for the protein solubilized in LMNG *vs.* DDM, as shown by F-NMR on labelled proteins [44]. Notably, it was proposed that this was related to the very low CMC of LMNG. From simple considerations, assuming that the on-rate for a monomer forming a micelle is diffusion-limited (thus related only to the detergent monomer size, similar for LMNG and DDM), the detergent off-rates are expected to be lower for LMNG than that for DDM, by a factor being the ratio of their CMCs [44] (the value of the CMC of LMNG will be discussed below). The large off-rate of LMNG may be an explanation for the slower protein dynamics. The fact that individual monomers dissociate much slower from the protein than other standard detergents would also explain the exceptional stabilization of protein-LMNG complexes, and the presence of residual activity measured after dilution below the CMC: LMNG "sticks" to the protein surface, and protein-detergent complexes are preserved. A protocol (GraDeR) was indeed proposed to prepare samples at 1 CMC of LMNG, thus devoid of excess LMNG, for obtaining cryo-electron microscopy images of significantly enhanced quality [47].

However, probably due to the particular geometry of this molecule, the LMNG detergent assemblies formed in solution may be rather large: a hydrodynamic radius of 7.2 nm was determined for a 0.5 % solution of LMNG [49]. The questions to be addressed are therefore: how are the large LMNG assemblies/micelles organized in solution? Does the large size of LMNG micelles lead to large protein-detergent complexes? What is the homogeneity and the quaternary structure of the solubilized membrane proteins, and how do they compare to those in more usual detergents? Is the crystallization process affected by the large size of the detergent micelles and/or the possible large size of the solubilized protein-detergent complexes?

To answer these questions, and having in mind that the effects of detergents are protein dependent, we characterized the assemblies in solution of LMNG alone and in complex with four different membrane proteins, FhuA, SpNOX, BmrA and bacteriorhodopsin (bR). We confirmed the stabilization propensity of LMNG compared to DDM, by measuring thermal denaturation by Differential Scanning Fluorimetry (DSF) of the four proteins, limited proteolysis of BmrA, and specific activities of BmrA and SpNOX. We also used complementary techniques such as small angle X-ray and Neutron scattering (SAXS and

SANS), Analytical Ultracentrifugation Sedimentation Velocity (AUC-SV) and Size exclusion chromatography coupled to light scattering (SEC-LS) and dynamic light scattering (DLS). We showed that, although LMNG alone forms increasingly large assemblies with increasing concentration, the protein-LMNG complexes are of comparable size to those formed with other detergents, with overall the same weight amount of bound detergent, and the oligomeric state of each protein remains unchanged. Furthermore, FhuA solubilized in LMNG showed an overall increased number of hits when screened for crystallization, suggesting that the large size of LMNG micelles does not prevent protein crystallization.

Materials and method

Chemicals and buffers

Detergents are from Anatrace, except octyl-β-D-thioglucopyranoside (OTG) from Acros, other chemicals are typically from Sigma-Aldrich.

Buffer A : 50 mM Tris-HCl pH 7.0, 300 mM NaCl

FhuA purification

FhuA was purified from the *E. coli* strain AW740 transformed with a plasmid encoding the *fhuA* gene in which a 6xHis tag has been inserted in the extracellular loop L5 [56]. Cells were grown in LB medium at 37 °C in the presence of 100 mM of the iron-chelating agent dipyridine, and broken with a microfluidizer (10 passages at 15 kpsi) in a 20 mM Tris-HCl pH 8, 150 mM NaCl buffer with a pinch of DNase I. Unbroken cells were removed by a first centrifugation (15 min, 6000 rpm, rotor SX4250), and the membrane fraction was recovered by ultracentrifugation (20 min, 35 000 rpm, 45Ti). A first solubilization with 2 % OPOE (octylpolyoxyethylene), 20 mM Tris-HCl pH 8.0, 30 min at 37 °C under gentle shaking solubilized the inner membranes, and the outer membrane pellet (20 min, 35 000 rpm, 45Ti) was solubilized in 1 % lauryldimethylamine-N-oxide (LDAO), 20 mM Tris-HCl pH 8, 1 mM EDTA for 1 h at 37 °C. Insoluble material was removed (20 min, 35 000 rpm, 45Ti). The protein was purified by Nickel affinity chromatography (HiTrap Chelating, 5 mL, GE Healthcare). The LDAO supernatant was supplemented with 5 mM $MgCl_2$ and 5 mM Imidazole, loaded onto the column and thoroughly washed (20 mM Tris-HCl pH 8, 150 mM NaCl, 0.1 % LDAO). A delipidation step was achieved by washing with 10 mL of the same buffer containing 1% LDAO. The protein was eluted with 20 mM Tris-HCl pH 8.0, 200 mM Imidazole, 0.1 % LDAO. Fractions containing the protein were pooled and loaded onto an anion-exchange chromatography (HiTrap Q, 1 mL, GE Healthcare) equilibrated with 20 mM Tris-HCl pH 8.0, 0.05 % LDAO and the protein was eluted by a linear gradient of NaCl in 20 mM Tris-HCl pH 8, 0.05 % (2.2 mM) LDAO (final NaCl concentration ~150 mM). The concentration of FhuA was determined using $\varepsilon_{280\ nm}$ = 103,690 M^{-1} cm^{-1}.

FhuA detergent exchange

For LDAO - LMNG exchange, the protein sample was diluted 50 times with water, to reach a detergent concentrations far below the LDAO CMC. Protein aggregation was checked by spectrometry (scattering), and the protein was recovered as a pellet by ultracentrifugation (20 min, 35 000 rpm, 45 Ti or 20 min, 80 000 rpm TLA 100.3 depending on the volume). The protein pellet was rinced with water, and resuspended in 11.9 mM LMNG, 20 mM Tris-HCl pH 8.0 to reach a final protein concentration of 7-10 mg mL^{-1}. A different protocol is described below for the thermal denaturation assays.

FhuA crystallization

Crystallization screening was carried out using commercial screens (Qiagen and Hampton Research). Sitting drops, consisting of 100 nL protein and 100 nL crystallization buffer, were

dispensed in 96-well plates (Greiner Crystal Quick plates) using a Cartesian PIXSYS 4200 robot (Genomic Solutions) and equilibrated at 20 °C against 100 mL of crystallization buffer. Hits were then manually reproduced and improved using the vapour diffusion hanging drop technique. The drops, consisting of 0.8 mL protein and 0.8 mL crystallization buffer, were equilibrated against 250 mL of crystallization buffer at 20 °C in 48-well plates (Hampton Research). Crystals were transferred to the crystallization buffer supplemented with 20% (v/v) glycerol for 30 s, flash-cooled and stored in liquid nitrogen.

FhuA LMNG data processing

The final data set was collected at 4 Å on beamline FIP-BM30A at the European Synchrotron Radiation Facility, Grenoble, France [57]. Data reduction was performed using the XDS program [58]. The space group was $C222_1$ (a = 149.53 Å, b = 210.96 Å, c = 188.70 Å) with two molecules per asymmetric unit (solvent content of 73 %). The structure was solved by molecular replacement performed with the Phaser program [59] using the model of the *E. coli* protein available in the Protein Data Bank (code 2FCP). A refinement was carried out with the *phenix.refine* program [60,61] in the 48-4 Å resolution range.

SpNOX production

SpNOX was overexpressed and purified in typically 0.025 mM LMNG, as previously described [62]. When using DDM as the detergent, the same purification protocol was used but with adjustments for DDM concentrations in the purification buffers corresponding to each step. Indeed, the solubilization step was performed using 5.1 mM DDM, the loaded Ni-HisTrap column was washed in the corresponding buffer containing 2 mM DDM, and eluted with 0.3 mM DDM in the elution buffer. Final size exclusion was performed in 50 mM Tris-HCl pH 7.0, 300 mM NaCl, 0.3 mM DDM.

BmrA production

Typical bacterial culture protocol: pET23b-*bmrA* [63] was used to transform C41(DE3) strain of *E. coli*. For preculture, 200 mL LB medium containing 100 µg mL^{-1} ampicillin was inoculated with a freshly transformed colony and growth allowed overnight at 37 °C and 180 rpm. The next morning, enough preculture was added into 1 L 2X YT medium, containg 100 µg mL^{-1} ampicillin, to get an optical density of 0.1, and growth then allowed at 37 °C 180 rpm. When the optical density reached 0.6, the culture was induced for the overexpression of BmrA for 4 h at 25 °C and 180 rpm by the addition of 0.7 mM IPTG (final concentration). Thereafter, the cells were harvested by centrifugation at 4,000 g at 4 °C for 20 min and the bacterial pellet was frozen at -80 °C until further use. Inverted Membrane Vesicles preparation : The bacterial pellet was resuspended in 50 mM Tris-HCl pH 8, 5 mM $MgCl_2$, 1 mM dithiotreitol, with an anti-protease cocktail from Roche. The bacterial cells were lysed by passing them thrice through Microfluidizer™ at 18,000 psi. Next, the cellular debris was removed by centrifugation at 15,000 g for 30 min at 4 °C. The membrane fraction was subsequently obtained by centrifugation at 150,000 g for 1 h at 4 °C. The membrane fraction was resuspended and centrifuged again, with the same conditions as before, after resuspension in 50 mM Tris-HCl pH 8, 1.5 mM EDTA, 1 mM dithiotreitol. Finally, the obtained membrane vesicles were resuspended in 20 mM Tris-HCl pH 8, 300 mM sucrose, 1 mM EDTA and flash frozen in liquid nitrogen before storage at -80 °C. The total protein concentration in membrane was analysed by BCA assay. BmrA purification: BmrA enriched Inverted Membrane Vesicles were solubilized for 1 h at 4 °C in 50 mM Tris-HCl pH 8, 10% glycerol, 100 mM NaCl, with 1% detergent (LMNG or DDM). The soluble fraction obtained after ultra-centrifugation, at 150,000 g for 1 h at 4 °C, was injected into a 1 mL HisTrap HP column (GE Healthcare) which was pre-equilibrated with the same buffer with 20 mM imidazole, and 0.1% (2 mM) DDM or 0.01% (0.1 mM) LMNG. The column was washed with

20 column volumes of the same buffer. Gradient elution was eventually performed with the same buffer with imidazole gradient from 20 mM to 500 mM. The protein fractions were dialyzed overnight at 4 °C against 50 mM Hepes pH 8, 10% glycerol, 50 mM NaCl, 2 mM DDM or 0.1 mM LMNG. The protein concentration, 2.2 mg mL^{-1} for both BmrA in 2 mM DDM and BmrA in 0.1 mM LMNG, was determined from UV absorbance at 280 nm by using Nanodrop spectrophotometer, and a $\varepsilon_{280\ nm}$ = 38850 M^{-1} cm^{-1}. Reconstitution of BmrA in proteoliposomes was performed as previously described [64].

Limited Proteolysis of BmrA

Apo form: Purified BmrA in detergent was added to buffer 50 mM Hepes-KOH pH 8, 50 mM NaCl, 10% glycerol and the specified detergent, in case of trypsin, or 100 mM ammonium bicarbonate pH 7.8 with the specified detergent, in case of protease V8. After 15 min of incubation, either trypsin (1 µg/250 µg of protein) or protease V8 (1 µg/20 µg of protein) was added. Samples of 10 µL (5 µg BmrA) were withdrawn at 0, 2, 5, 15, 30, 60, 120, 180 and 300 minutes. 2.5 µL of TFA 5% was added immediately to each sample to stop the reaction. 3 µL of Laemmli 5x was then added and the samples were placed in ice before resolving them on SDS-PAGE. Vanadate-inhibited form: For the Vi-inhibited form, before the addition of purified BmrA, the buffer was supplemented with 3 mM $MgCl_2$, 2 mM ATP and 1 mM Vi. The samples were then incubated for 15 min before the addition of protease. Samples of 10 µL were withdrawn and treated thereafter in the same way as the apo form.

bR solubilization and detergent exchange by sucrose gradient

Purified purple membrane was solubilized for 40 h at 4 °C with 89 mM OTG (CMC = 9 mM) at a membrane concentration of 1.5 g L^{-1} in 20 mM sodium phosphate buffer, pH 6.8. Samples were diluted to reach a final OTG concentration of 15 mM, supplemented with 2 mM of the surfactant to be tested, and incubated 15 min prior to being loaded onto a 10–30 % (w/w) sucrose gradient containing 20 mM sodium phosphate buffer pH 6.8 and 0.2, 2 or 20 mM LMNG. A control gradient contained 1 mM DDM. Gradients were centrifuged for 15 h at 55,000 rpm (200,000 g) in the TLS55 rotor of a TL100 ultracentrifuge (Beckman). Bands containing the colored protein were collected with a syringe, and protein samples were kept at 4 °C in the dark for UV-visible spectrophotometry. To check for detergent exchange, 10 µl of each recovered bR band was deposited onto a Thin Layer Chromatography (TLC) silica plate (Macherey-Nagel, ref. 818423), and migration performed in a Chloroform/Methanol/Water solvent (65/35/5). After drying, the plate was first stained with iodine vapour and then with orcinol (0.1 % orcinol in 3 % H_2SO_4 and 72.5% ethanol) and charring at 120 °C.

Thermal denaturation and activity assays

Thermal unfolding experiments and analysis were performed by differential scanning fluorimetry coupled to back scattering using a Prometheus NT.48 instrument (Nanotemper Technologies, Munich, DE), and the provided software PR.thermocontrol v2.0.4. Up to 48 capillary containing 10 µL of sample are sequentially illuminated at 280 nm, and fluorescence intensity at 350 (F350) and 330 (F330) nm, and back scattering measured as a function of temperature. The derivatives of F350/F330 and of the back scattering were used to estimate the melting temperature, T_m, and the onset of aggregation, T_{agg}, respectively. For FhuA : samples were prepared by diluting 48 times a stock sample of 1.92 mg mL^{-1} FhuA, in 2.2 mM LDAO, 20 mM Tris pH 8.0, ~150 mM NaCl, into 20 mM Tris pH 8.0 with the appropriate detergent, leading to a final residual LDAO concentration of ≈ 0.05 mM (0.05 CMC), with FhuA at 0.04 mg mL^{-1}. For SpNOX : samples were prepared after purification in LMNG, and eventual detergent exchange in DDM, and concentration. Buffer is 50mM Tris HCl pH 7.0, 300 mM NaCl, 10 µM FAD, with 0.025 mM LMNG or 0.2 mM DDM initial concentrations,

0.21 LMNG and 1.27 mM DDM final estimated concentrations, considering co-concentration of protein and detergent, and SpNOX at 8.3 mg mL^{-1}, in the T_m assays. For activity assays, SpNOX was diluted to 1 µg mL^{-1} in 50 mM Tris HCl pH 7.0, 300 mM NaCl, 10 µM FAD , with 0.025 mM LMNG or 0.2 mM DDM. Activity assays were performed in the presence of 100 µM Cytochrome C, 10 µM FAD, 200 µM NADPH, following Cytochrome C absorbance at 550 nm. For BmrA : for T_m measurements, samples were prepared at a final protein concentration of 1 mg mL^{-1}, from dilution of the purified protein in 50 mM Hepes pH 8, 10% glycerol, 50 mM NaCl, with 2 mM DDM or 0.1 mM LMNG. For Vi-inhibited form of BmrA, the dilution buffer also contained 10 mM ATP, 10 mM $MgCl_2$ and 1 mM Vi (all final concentrations). BmrA samples were incubated for 15 min at room temperature before allowing them to be filled in the capillaries for Nano DSF analysis. The activity assays of BmrA were done in a quartz cuvette with a final volume of 700 µL. The buffer, containing 50 mM Hepes/KOH pH 8, 10 mM $MgCl_2$, 4 mM phosphoenolpyruvate, 0.3 mM NADH, 32 µg mL^{-1} lactate dehydrogenase, 60 µg mL^{-1} pyruvate kinase, 10 mM ATP and either 2 mM DDM or 0.1 mM LMNG, was added into the cuvette and was allowed to attain the desired temperature i.e. 37 °C for 5 min, before adding 3 µg protein, and measuring the absorbance at 340 nm for 20 min at 37 °C. For bR : to perform T_m measurements, after the solubilization step (see above), solubilized bR was incubated 40 mins at 4 °C in the presence of biobeads (10 g/g OTG), that reduced the concentration of OTG to 70 mM estimated from TLC, from the comparison with OTG aqueous solution at 10, 25, 50, 75 and 100 mM. TLC was performed as described above in bR preparation, but the mobile phase was Chloroform/Methanol 2/1, and the volume deposited was 1 µL. Imaging and quantification were done with the Gel Doc XR system and Image lab software (Biorad). The bR was then diluted 18 times in 0.1 M NaCl, 0.02 M Na phosphate buffer supplemented with the appropriate detergent, residual OTG concentration being estimated as 0.4 its CMC, and final bR concentration to 0.14 mg mL^{-1}. In the thermal denaturation assays, the temperature was increased by 1 (FhuA, bR, SpNOX) or 0.5 (BmrA) °C/min from 15 °C (FhuA, bR, SpNOX) or 20 °C (BmrA) up to 95 °C.

Density measurements

31.8 mg of dried LMNG was dissolved in 1.99948 g of water. From the density of water (0.998205 +/- 0.000001 g mL^{-1}) and sample (1.001416 +/- 0.000002 g mL^{-1}) determined from triplicate measurements at 20 °C using a DMA 58 density meter (Anton Paar, Graz, Austria), we derived [65] a LMNG concentration of 15.68 mg mL^{-1} and a partial specific volume $\bar{v}$ = 0.797 mL g^{-1}.

AUC-SV

AUC-SV experiments were conducted in an XLI analytical ultracentrifuge (Beckman, Palo Alto, CA) using an ANTi-50 rotor, using double channel Ti centre pieces (Nanolytics, Germany) of 12, 3, or 1.5 mm optical path length equipped with sapphire windows, with the reference channel being typically filled with solvent without detergent. For BmrA, LMNG was in the buffer in the reference channel, and we used double sector capillary type cells (Beckman, Palo Alto, CA) allowing perfect matching of the channel heights upon centrifugation 90 min at 7,000 rpm (3,600 g). Acquisition was done at 42,000 rpm (130,000 g), overnight, using absorbance (280 nm, and additionally for SpNOX, 412nm) and interference detection. Data processing and analysis was done using the program SEDFIT [66] from P. Schuck (NIH, USA), REDATE [67] and GUSSI [68] from C. Brautigam (USA), and using standard equations and protocols described in [65,69–71]. LMNG samples in water were prepared from precise weight dilution from a stock solution at 9.88 mM. The sedimentation velocity profiles for LMNG at 23.2 and 35 mM in Buffer FhuA showed an

optical artefact, and *s*-values were determined from $(r_b/r_m)=s\omega^2t$, with r_b the radial position at half the plateau signal, r_m the meniscus position, ω the angular velocity, and t the time. Corrected *s*-values for solvent density and viscosity, s_{20w}, are calculated, for membrane proteins, considering for their partial specific volume, the mean value between protein and detergent.

Dynamic light scattering (DLS) of LMNG

LMNG at 20 mM in water was measured using the DynaPro NANOSTAR (Wyatt, Santa-Barbara, USA) instrument, at room temperature, and analyzed with the associated software DYNAMICS.

SEC-LS

SEC-LS experiments were conducted at 4 or 6 °C on a HPLC consisting of a degasser DGU-20AD, a LC-20AD pump, an autosampler SIL20-AC_{HT}, a communication interface CBM-20A and a UV-Vis detector SPD-M20A (Schimadzu, Kyoto, Japan), a column oven XL-Therm (WynSep, Sainte Foy d'Aigrefeuille, France), a static light scattering miniDawn Treos, a dynamic light scattering DynaPro NANOSTAR, and a refractive index Optilab rEX detectors. The analysis was made with the software ASTRA, v5.4.3.20 (Wyatt, Santa-Barbara, USA). Samples of 10 to 60 µL were injected at 0.5 mL min^{-1} on a Superdex 200 10/300 GL (GE Heathcare), equilibrated with the elution buffer. Bovine serum albumin at 2 mg mL^{-1} in PBS buffer was injected as a control in each experiment. The extinction coefficient and refractive index increments for the proteins were calculated from the amino-acid sequences using the program SEDFIT described above. For LMNG, we used $\partial n/\partial c$=0.146 mL g^{-1} determined by AUC.

SAXS and SANS samples

A first series of SAXS measurements was carried out with 14 samples of LMNG in H_2O, at concentrations between 0.31 and 20 mM, and a second series, measured by SAXS and SANS, with four samples of LMNG in H_2O and in D_2O, at 20 and 10 mM. SANS contrast variation determination was achieved for LMNG at 20 mM in 25 mM Tris pH 8, 150 mM NaCl, 10% glycerol, with different D_2O %s. LMNG concentrations were precisely determined using weighing-controlled solubilization and dilutions.

SAXS experiment

SAXS experiments were conducted on the BM29 beamline at the European Synchrotron Radiation Facility (Grenoble, France). The data were recorded for $0.004<Q<0.5$ $Å^{-1}$ ($Q=(4\pi/\lambda)\sin\Theta$ is the modulus of the scattering vector, with 2Θ being the scattering angle, and λ the wavelength), using a two-dimensional 1M Pilatus detector, at 20 °C, with a monochromatic X-ray beam with λ = 0.9919 Å and a sample to detector distance of 2.864 m. Measurements were performed with 50 µL loaded sample, in a quartz capillary, with a continuous flow. In the first series, 10 acquisitions with 1 s irradiation per acquisition (flow of 2.7 µL/s), in the second series, 10 and 30 acquisitions with 0.5 s irradiation (flows of 5 and 1 µL/s), were recorded for the samples and the solvents. The scattering curves were indistinguishable with the two flows. Data reduction was performed using the automated standard beamline software (BSxCuBE) [72], and data processing, including the elimination of data suffering from radiation damage, averaging, buffer subtraction, Guinier plots, using PRIMUS of the software suite ATSAS [73]. Absolute scales were obtained using the scattering of water.

SANS experiment

SANS experiments were carried out on the small-angle diffractometer D22 at the Institut Laue Langevin (Grenoble, France), at 20 °C, using neutron wavelengths λ of 6 and 12 Å, with samples measured in Hellma quartz cells 100QS with 1-mm optical path length. Scattering data for LMNG at 10 and 20 mM in H_2O and D_2O were recorded at 20 °C for $0.003 < Q < 0.45$ Å^{-1}, using a neutron wavelength λ of 6 Å, and sample-detector/collimation distances (SD / coll) of 17.6 m / 17.6 m, 5.6 m / 5.6 m, and 1.4 m / 2.8 m for 15, 5 and 5 mins, respectively. For LMNG at 20 mM in D_2O, additional data were recorded at (SD/coll) of 17.6 m / 17.6 m at 12 Å, leading to a total *Q*-range of 0.0012-0.45 Å^{-1}.Transmissions were measured at 17 m for 1 min. For the determination of the contrast match point, samples were measured at 10 °C, with SD / coll of 5.6 m / 5.6 m, 1.4 m / 2.8 m, for 5 and 1 min. respectively, and transmissions were measured at 5.6 m for 1 min. LMNG at its match point, in 21.4 % D_2O, was measured at 15 °C, with SD / coll of 8 m / 8 m and 1.4 m / 2 m for 60 and 15 min, respectively. Data reduction to obtain scattering curves in absolute scale, and manipulation -merging, buffer subtraction- were done in the usual way (see *e.g.*[74]) using Grasp (a Matlab™ script application produced by ILL) and SANS reduction macros provided by NIST Center running on IGOR (Wavemetrics)[75]. Absolute intensities are obtained using the direct beam measurement.

SAXS and SANS Guinier analysis

The radii of gyration (*R*g) and the intensities scattered in the forward direction (*I*(0)) were extracted by the Guinier approximation, with $RgQ \leq 1.3$. Aggregation number were derived from the molar mass of LMNG micelle, *M* (g mol-1) obtained from the absolute forward intensity, *I*(0) (cm^{-1}), using $M = (I(0)/c)N_A/(\partial\rho_{el}/\partial c)^2$, in SAXS, and $M = (I(0)/c)N_A/(\partial\rho_N/\partial c)^2$, in SANS. N_A is Avogadro's number, *c* the concentration (g mL^{-1}), and $\partial\rho_{el}/\partial c$ and $\partial\rho_N/\partial$c (cm g^{-1}) the increment of electron and neutron, respectively, scattering length density per g of LMNG. $\partial\rho_{el}/\partial c = (\rho_{el} - \rho^\circ_{el})\, r_{el}\ \bar{v}$, with $\rho_{el} = 4.105\ 10^{23}$ (from composition and $\bar{v}$) and $\rho^\circ_{el} = 3.297\ 10^{23}$ the numbers of electron per mL of LMNG and solvent, respectively, and $\rho_{el} = 2.818\ 10^{-13}$ cm the scattering length of an electron. $\partial\rho_N/\partial$c was calculated to be $1.108\ 10^{10}$ cm g^{-1} in H_2O, and $-3.509\ 10^{10}$ cm g^{-1} in D_2O.

SAXS and SANS combined analysis for LMNG shape

SAXS and SANS data were analyzed using shape-dependent models in SASview [76]. The scattered intensity from an homogeneous dispersion of particles is written as:

$$I(Q) = N\,V^2\,(\Delta\rho)^2\,P(Q)\,S(Q)$$

Where *N* is the number density of particles, *V* their volume, $\Delta\rho$ (cm^{-2}) is the scattering contrast, *P*(*Q*) is the inter particle form factor and *S*(*Q*) is the interparticle structure factor.

In the present case, SAXS and SANS data have been fitted simultaneously with a core shell cylinder form factor and hard sphere potential with beta approximation using SASview software. The cylinder form factor included size polydispersity on radius (fixed at 5 %) using a gaussian distribution. The scale factor was fixed by the surfactant concentration. The head groups SLD or ED were fitted using the same hydration level of the anhydrous polar hear. Radius, length and shell thickness of the cylinder were constrained and kept equal for X-ray and neutrons. Fitting was performed using the optimizer DREAM which allows to set simultaneous fits as well as proper error determination.

Results

Hydrodynamic characterization of LMNG

Our first aim was to characterize the assembly properties of LMNG molecules by itself. AUC-SV experiments were done for LMNG solubilized in water at different concentrations. The SV profiles and analysis in terms of continuous distributions $c(s_{20w})$ of sedimentation coefficients, s_{20w}, showed a unique or main boundary. The mean s_{20w}- value increased with concentration, from 3.3 S at 0.25 mM to 7.9 S at 9.8 mM (Fig 1A-C). This indicates that LMNG micelle aggregation number increases with concentration, an atypical behaviour compared to usual detergents. Complementary AUC-SV in a dilute buffer (20 mM Tris-HCl pH 8.0, 150 mM NaCl), at larger LMNG concentrations of 23 and 35 mM, gave estimates for s_{20w} of 7.7 and 8.7S, respectively. By integrating the signal for the micelles at the different LMNG concentrations (Fig 1D), we determine, in water, a refractive index increment for LMNG $\partial n/\partial c$=0.146 mL g^{-1} (close to that of DDM, 0.143 mL g^{-1} [65]), and a CMC of 40 µM. The knowledge of the partial specific volume, $\bar{v}$, of LMNG is required to correlate s_{20w} and molar mass, or aggregation numbers $N_{agg.}$ We measured, with density measurement, $\bar{v}$ = 0.797 mL g^{-1}, a value close to that of DDM: 0.82 mL g^{-1} from [65] and 0.81-0.837 mL g^{-1} from [1].

Minimum aggregation numbers N_{agg} of 63 and 230 are calculated at 0.25 and 10 mM considering globular compact micelles (frictional ratio of 1.25), but N_{agg} are larger, at least for the larger micelles, since their shape is anisotropic (see below). Dynamic light scattering (DLS) of 20 mM LMNG in water showed essentially one population with a polydispersity index of 35% and a hydrodynamic radius, R_H, of 14 nm (Fig 1E), in line with the reported value of 7.2 nm at 5 mM [49]. Combining s_{20w} and R_H values at 5 and 20 mM provides N_{agg} estimates of 300 and 620, corresponding to frictional ratios of 1.65 and 2.4, indicating moderately and strongly elongated shapes, respectively.

In SEC-LS experiments with 0.05 mM LMNG in the equilibration and elution buffer (bufferA), LMNG injected at 2, 5, 10 and 20 mM eluted as a very large peak covering the elution volumes of BSA monomer (65 kDa) to BSA trimer (Fig 1F). When LMNG concentration increased, the elution volume decreased. However, the molar masses determined from coupled refractive index and light scattering detections did not change significantly, neither along the elution, nor with the injected LMNG concentration: from 67 kDa (N_{agg} = 67) at 2 mM to 76 kDa (N_{agg} = 76) at 20 mM (Fig 1F). This suggests the dissociation of the largest LMNG complexes upon sample dilution on the column.

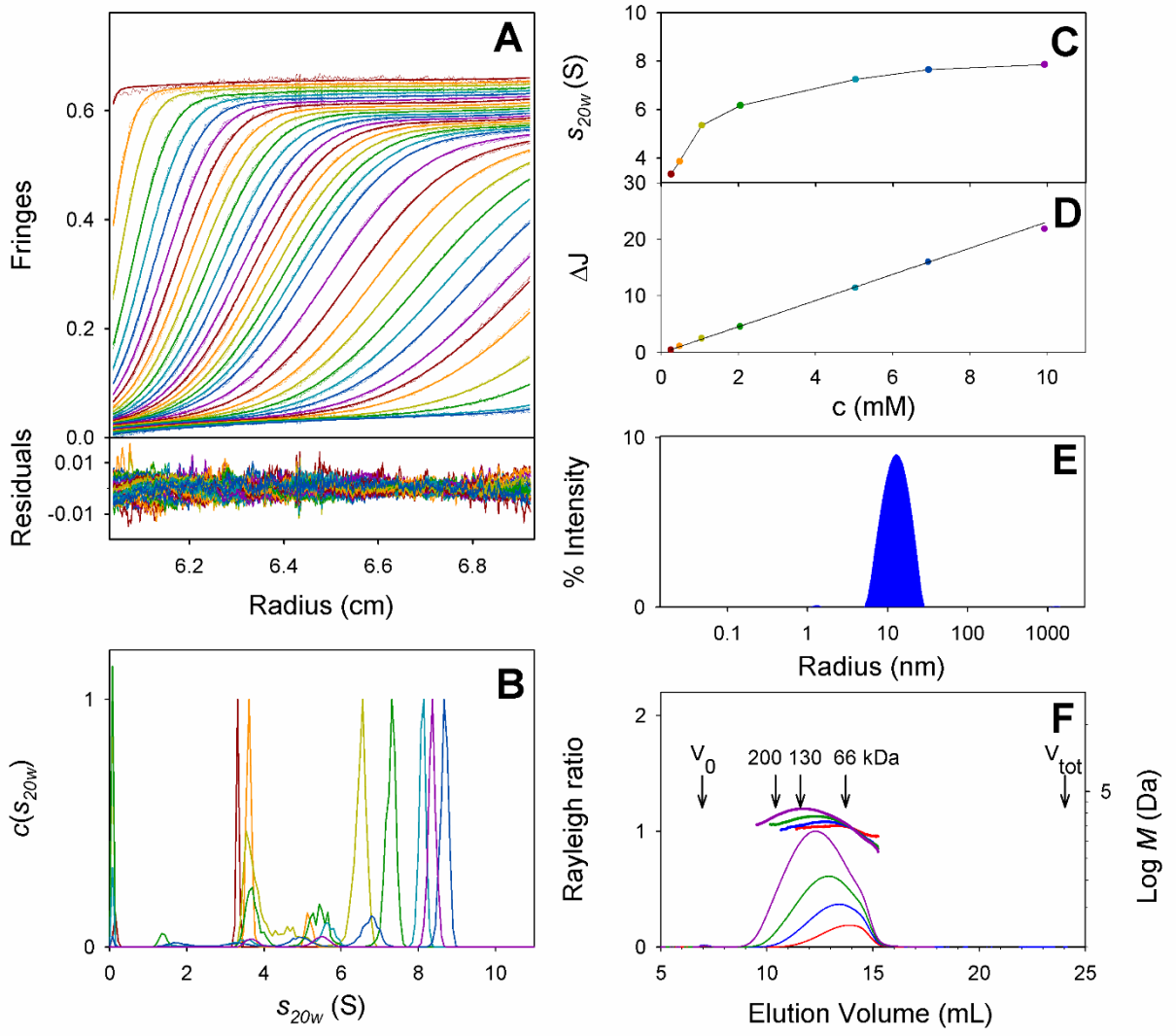

Fig 1. LMNG in AUC-SV, DLS, and SEC-LS

AUC-SV: **A**: Superposition of experimental and fitted sedimentation velocity profiles (top) and residuals (bottom), obtained at 130,000 g and 20 °C during ≈ 5 hours using interference optics and 12 mm optical path centerpiece, for LMNG at 0.25 mM in water. **B**: Superposition of the normalized *c*(*s*) distributions for LMNG at 0.25 (brown), 0.5 (orange), 1 (yellow-green), 2 (green), 5 (cyan), 7 (blue), and 10 (purple) mM. **C**: plot of the mean sedimentation coefficient s_{20w} *versus* LMNG concentration. Note that the mean s_{20w} is obtained from the intergration of the $c(s_{20w})$ over the whole s_{20w}- range; At 10 mM compared to 7 mM, as seen in Panel B, s_{20w} the for the main species is decreased, while, as seen in Panel C, the mean s_{20w} is slightly increased. **D**: Fringe number Δ*J*, normalized to 1 cm optical path-length, for the micelle contributions *vs* total LMNG concentration, and linear fit. DLS: **E**: Hydrodynamic radius distribution of LMNG at 20 mM in water. SEC-LS: **F**: Rayleigh ratio measured along the elution profiles, for 30 µL LMNG injected at 2, 5, 10, and 20 mM (red, blue, green, and purple thin lines, respectively) on a Superdex 200 10/300 GL (GE Heathcare) column eluted with 50 mM Tris-HCl pH 7.0, 300 mM NaCl, 0.05 mM LMNG, and molar masses (thick lines, right axis) derived from the light scattering and refractive index detections. V_0 is the dead volume, V_{tot} the total volume of the column, and the arrows indicate the elution volumes of BSA as a monomer, dimer, and trimer (66, 130, and 200 kDa) from a different injection.

Structural characterization of LMNG by small angle scattering

SAXS and SANS experiments were performed to get additional information on the size and shape of LMNG micelles. A first set of SAXS experiments were done with LMNG between 0.3 and 20 mM (0.03 and 2%) (Fig 2A). From the Guinier analysis, the size of the micelle increases with *R*g and aggregation numbers increasing from 3.4 nm to 10 nm, and from 55 to 240, respectively, when LMNG concentration is raised from 0.3 to 10 mM. (Fig 2B and 2C).

These values remain constant for LMNG concentrations increasing from 10 to 20 mM, and indeed the scattering curves are superimposed (Fig 2A). All curves are superimposed at the largest angles, representing the smallest distances in the real space, compatible with a circular cross section. To ascertain the shape of the LMNG micelles, 10 and 20 mM LMNG samples were measured by SAXS and SANS, in H_2O and D_2O. In the same buffer, the scattering curves normalized by concentration were superimposable for the 10 and 20 mM LMNG samples. From Guinier plots, the radii of gyration from SAXS were 11.5 and 11.6 nm at 10 and 20 mM in H_2O, and 17.7 and 17.2 nm at 10 and 20 mM in D_2O. The aggregation numbers were 285 in H_2O, and 528 in D_2O. The *R*g and aggregation numbers from SAXS, in H_2O were slightly larger but similar to those of the first set of experiments. The size of the micelles appears significantly larger here for LMNG in D_2O than in H_2O, but, as will be discussed below, the significance of this difference is not ascertained.

The SAXS and SANS scattering curves of 20 mM LMNG in H_2O and D_2O were analyzed globally. We used a model of a core shell cylinder with hard sphere interaction, defined by a core representing the hydrophobic tails (*i.e.* the hydrocarbon chains) covered by a shell representing the hydrated polar heads. The scattering length densites (SLD) of the core and of the solvent were fixed to the theoretical values. The SLD of the polar head (different in SAXS and SANS), and the dimensions of the micelles (radius of the cylinder core, thickness of the shell, and length, common in SAXS and SANS) were globally fitted keeping the same hydration level in X-ray and neutron. The results are presented in Table 1. The fitted values for the SLD of the anhydrous shell values are in the same order of magnitude as those calculated for the anhydrous polar head. We extracted reasonable hydration of 30 % in H_2O and 44 % in D_2O. The radius of the hydrophobic core, 14 Å, and that of the shell thickness, 7-9 Å, are in line with those expected from the LMNG size.

Finally, we investigated whether LMNG could be totally matched out in SANS. This is required to be able to focus on protein contribution. The differential distribution of detergent hydrophobic tails and hydrophilic heads in the detergent micelles and bound detergent indeed corresponds to ordered scattering density fluctuations, which makes the scattering curve of the micelles and bound detergent possibly not flat even at the match point [77]. We thus measured for LMNG a set of contrast variation curves, using a solvent with different %s of D_2O. We determined a contrast match point of 21.4 % D_2O (Fig 2F). The scattering curve of the 2 mM LMNG sample in 21.4 % D_2O perfectly superimposes that of the solvent (Fig 2G). Thus LMNG can be homogeneously masked. The analysis of the neutron scattering curves of membrane proteins solubilized in LMNG, in 21.4 % D_2O will not require the fastidious step of detergent modelling to access membrane protein envelope structure. Because the contrast match point of hydrogenated proteins is ≈ 44 % D_2O, membrane proteins should be deuterated to improve their scattering signal, but this is not problematic, since deuterating proteins, in general, is not an issue.

To summarise, SAXS and SANS showed that LMNG forms large elongated rod-like micelles above the mM concentration. Given this observation, the question of the homogeneity of different membrane proteins at various LMNG concentrations was addressed below.

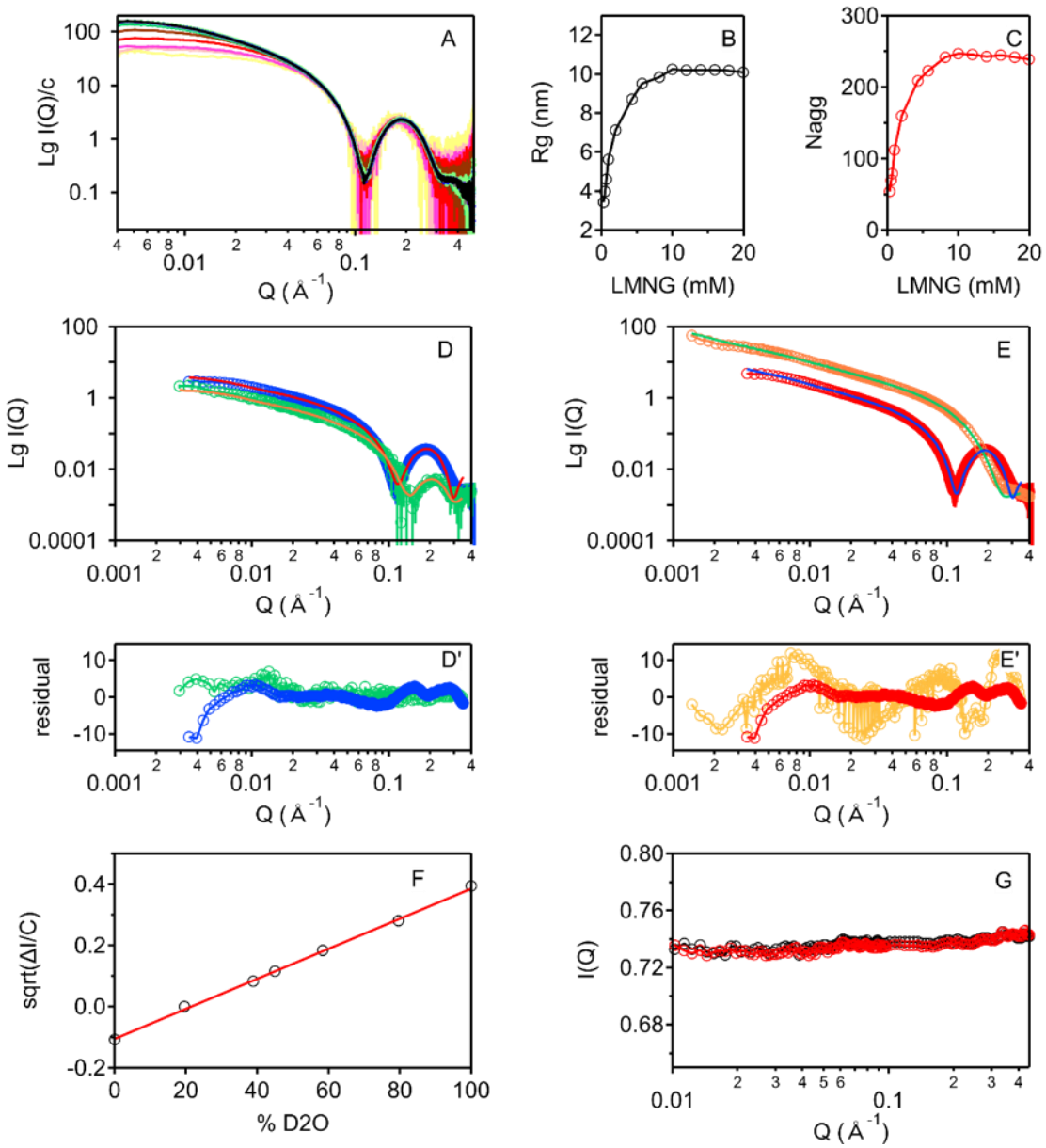

Fig 2. SAXS and SANS analysis of LMNG

A: Superposition of 13 SAXS profiles obtained at 0.3 (yellow), 0.5 (pale pink), 0.7 (pink), 1 (red), 2 (brown), 6 (green), 8 (light green), 10 (light blue), 12 (blue), 14 (navy), 16 (purple), 18 (grey), and 20 (black) mM LMNG, in H_2O, at 10 °C. **B**: corresponding *R*g, and, **C**: aggregation numbers, versus LMNG concentrations. **D,E**: Superposition, for LMNG at 20 mM in H_2O (D), and D_2O (E) of the experimental scattering curves obtained by SAXS (blue and red dots, respectively) and SANS (green and orange dots, respectively), and of the fitted curves, in the model of a core-shell cylinder, in SAXS (red and blue lines in H_2O and D_2O, respectively), and in SANS (orange and green lines lines in H_2O and D_2O, respectively); **D',E'**: respective normalized by data error residuals. SAXS and SANS data in each solvent were globally fitted (Table 1). **F:** Match point determination from SANS scattering curves obtained for 20 mM LMNG in 0, 20, 40, 45, 60, 80, and 100 % D_2O. **G:** Superposition of raw scattering curves obtained in a solvent with 21.4 % D_2O for LMNG at 2 mM (black) and of the solvent alone (red).

Table 1. Rod analysis of SAXS and SANS data for 20 mM LMNG

	LMNG 20 mM in H_2O		LMNG 20 mM in D_2O	
	SAXS	*SANS*	*SAXS*	*SANS*
Q range ($Å^{-1}$)	0.0035-0.35	0.0030-0.35	0.0035-0.35	0.0015-0.35
χ^2_R	3.2	3.2	2.3	26.7
Background, fixed (cm^{-1})	0.0008	0.001	0.0012	0.0015
SLD solvent, fixed (10^{-6} $Å^{-2}$)	9.4	-0.56	9.4	6.4
SLD core, fixed (10^{-6} $Å^{-2}$)	8.3	-0.3	8.3	-0.3
SLD shell, fixed (10^{-6} $Å^{-2}$)	14.75	1.88	14.75	3.99
SLD shell, fitted (10^{-6} $Å^{-2}$)	13.12+/-0.02	1.134*	12.42+/-0.02	5.048*
Fitted shell hydration (%)	30		44	
Radius (Å)**	14.51 ± 0.02		13.29 ± 0.01	
Thickness (Å)	7.33 ± 0.04		9.25 ± 0.03	
Length (Å)	603 ± 7		5376 ± 16	
Vol fraction	0.02 ± 0.00001		0.01951 ± 0.00006	

χ^2_R: reduced χ^2. *: linked parameter. **: a polydispersity on radius width was fixed to 5%.

FhuA-LMNG assemblies

FhuA is an *E. coli* outer membrane ferrichome-iron transporter involved in bacteriophage infection [78,79]. The structure of this robust β-barrel protein was solved in 1998 [80]. We investigated FhuA stability, homogeneity and association state at different LMNG concentrations, and whether the protein can crystallize in LMNG.

We first compared the thermal stability of FhuA in LDAO and in LMNG by DSF, allowing to measure the melting temperature (T_m) of the protein by probing the fluorescence emission (F_{350nm}/F_{330nm} ratio) of the aromatic residues upon increasing temperature. Simultaneous light back-reflection measurements permit to detect qualitatively aggregation events. Detergent was exchanged by a 48 times dilution, leading to a final residual concentration of LDAO that was much below its CMC (20 times). The melting curves are similar whatever the final detergent concentration, corresponding to CMC + 0.2, 0.5 mM and 1-2 mM, *i.e*. LDAO at 1.2, 1.5, and 2.2 mM and LMNG at 0.21, 0.51 and 2.01 mM. They show (Fig 3A) two unfolding events, attributed to, first, the unfolding of the cork, and then of the barrel [81] (both domains contain tryptophans). From light back-reflection, the onset of protein aggregation coincides with the first T_m, and significant aggregation to the second T_m. In LDAO, the T_m at 63 and 69 °C are in line with the published values of 60-65 and 74-75 °C, from scanning calorimetry [81], or synchrotron radiation circular dichroism [78] in slightly different buffers with 1.3 or 4.4 mM LDAO. In LMNG, unfolding is shifted to higher temperatures. The first T_m is at 67 °C, showing a moderate stabilization (+ 4 °C) of the cork, the second one at 80 °C indicating a significant stabilization (+ 11°C) of the barrel. T_m values are reported in Table 2. For comparison, binding of ferrichrome, the natural ligand, was described to have a strong stabilizing effect on FhuA cork, shifting the first transition by 6 °C [81]; binding of phage T5 Receptor Binding Protein pb5 leads to one unique unfolding event at 89 °C (+ 15 °C vs T_m of barrel for FhuA alone) [78]. Thus, LMNG significantly stabilizes both the flexible parts and the rigid domain of this β-barrel protein.

Table 2. Melting temperatures of FhuA, SpNOX, BmrA, and bR

Protein	Detergent type	detergent conc. (mM)	Micelle conc. (mM)		T_m (°C)	T_{agg} (°C)
FhuA	LDAO	1.2, 1.5, 2.2	0.2, 0.5, 1.2		63.0 + 69.0	65
FhuA	LMNG	0.21, 0.51, 2.0	0.2, 0.5, 1.0		67.0 + 80.0	74
SpNOX	DDM	1,27	1.1	40.5	56	
SpNOX	LMNG	0.21	0.2	53.9	60	
BmrA Apo	DDM	2	1.8	41.2	54	
BmrA Apo	LMNG	0.1	0.1	45.7	70	
BmrA Vi-inh	DDM	2	1.8	46.4	45	
BmrA Vi-inh	LMNG	0.1	0.1	59.3	50	
bR	OTG	11	2.0	53.6	43	
bR	DDM	2.01	1.8	59.9	52	
bR	LMNG	2.17	2.2	65.9	63	

T_m: melting temperature measured by differential scanning fluorimetry; T_{agg}: onset temperature for aggregation from light back reflexion. BmrA Vi-inh, Vi-inhibited forms were incubated with 10 mM ATP, 10 mM $MgCl_2$, and 1 mM vanadate. Standard deviations of typically 0.2 were determined from triplicates experiments in BmrA, otherwise the precision on T_m is estimated at 1°C. Micelle concentrations (*i.e.* above the CMC concentrations) were calculated considering CMC-values of 1, 0.01, 0.17 and 9 mM for LDAO, LMNG, DDM, and OTG, respectively.

For FhuA, detergent exchange can easily be done, by dilution of the purified protein solution until FhuA precipitates and re-solubilization of the pellet in the desired detergent. The resulting sample in LMNG, also used for crystallization assays, contained ≈ 7.5 mg mL^{-1} FhuA and 12 mM (total concentration) LMNG. SV-AUC analysis shows a main contribution (≈ 75% of the absorbance) at s_{20w} = 7.8 S, *i.e.* the same value as that published for FhuA in DDM [82]. Additional contributions are detected at s_{20w} = 10.7 S (≈ 5%) and 6.2 S (15-20%), which correspond reasonably to FhuA dimer and LMNG free micelles, respectively (Fig 4AB). Analysis of the absorbance of interference fringe signals provides an estimate of 1 g g^{-1} (80 mol mol^{-1}) of bound LMNG, and a free micelle concentration of 4.5 mM. In order to investigate the effect of LMNG concentration on FhuA homogeneity, complementary SV-AUC experiments were done on a similarly prepared sample with nominal concentrations of 5.4 mg mL^{-1} FhuA and 13 mM LMNG, and two derived samples, with FhuA diluted twice, and increased LMNG nominal concentrations to 18 and 24 mM. For these three samples too, only one main boundary is observed (> 80%) at about 7 S (Table 3). Probably, due to the large total concentrations of LMNG and FhuA, the fit is poor and the s_{20w} values imprecise (data not shown). The data can be interpreted by the non-ideal co-sedimentation of FhuA complexes and of LMNG free micelles, sedimenting at nearly the same s_{20w} value (Table 3). Nevertheless the membrane protein appears to remain monomeric in the presence of even very large concentrations of LMNG, where the latter forms large micelles. SEC-LS performed on a similar sample injected after 10 times dilution, showed traces of aggregates, FhuA dimer as a shoulder, FhuA monomer as the main contribution at 12.3 mL, and LMNG micelles at 14.5 mL (Fig 4C). The molar mass analysis gives for the main peak 79.3 kDa for FhuA molar mass contribution, in agreement with the protein sequence (79.9 kDa), and 98.5 kDa for LMNG contribution, corresponding to 1.2 g g^{-1} (95 mol mol^{-1}) bound detergent.

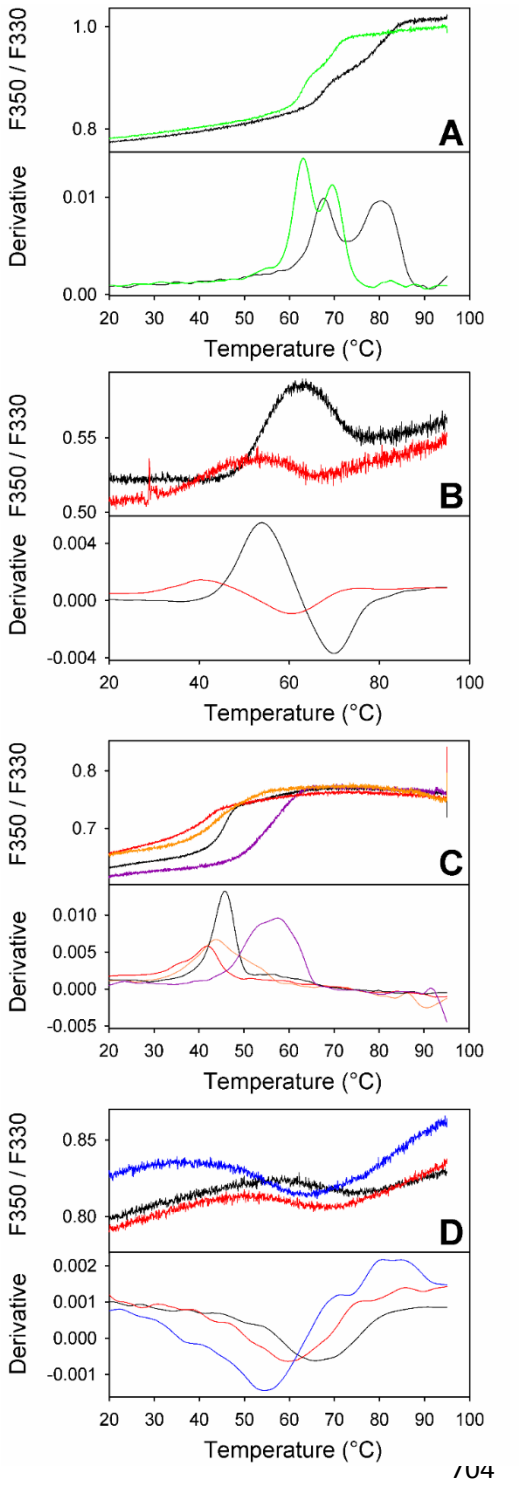

Fig 3. Thermal denaturation of FhuA, SpNOX, BmrA, and bR, by differential scanning fluorimetry
Ratio of the fluorescence emitted at 350 and 330 nm (top panels), and derivative (bottom panels) for **A:** FhuA at 0.04 mg mL^{-1} in the presence of LDAO 1.2 mM (green) or LMNG 0.21 mM (black); **B:** SpNOX at 8.3 mg mL^{-1} in the presence of DDM 1.27 mM (red) or LMNG 0.21 mM (black); **C:** BmrA at 1 mg mL^{-1}, in DDM 2 mM, in the Apo (red), or Vi-inhibited (orange) forms, and in LMNG 0.1 mM, in the Apo (black), or Vi-inhibited (purple) forms. The Vi-inhibited forms were incubated with 1 mM Vi, 10 mM ATP and 10 mM $MgCl_2$ for 15 minutes. **D:** bR at 0.14 mg mL^{-1} in OTG 11 mM (blue), DDM 2.17 mM (red), or LMNG 0.21 mM (black).

704

705
706
707

Table 3. LMNG solubilized FhuA in AUC-SV

exp	FhuA (mg mL^{-1})	total LMNG (mM)	free LMNG[a] (mM)	Main s_{20w} (S) from A_{280}[b]	Main s_{20w} (S) from ΔJ[b]	s_{20w} (S) for LMNG[c]
1	7.5	12	4.5	7.8	7.8	6.8
2	5.4	13	7.6	6.8	6.8	7.6
3	2.7	18	15.3	6.4	7.1	7.6
4	2.7	24	21.3	7.0	7.5	7.7

LMNG free micelles and FhuA complexes sediment separately (Fig 4) in exp 1, but are not resolved in exp 2-4. [a]calculated with the hypothesis of 1 g g^{-1} LMNG bound to FhuA, except for exp. 1, where free LMNG micelle concentration was

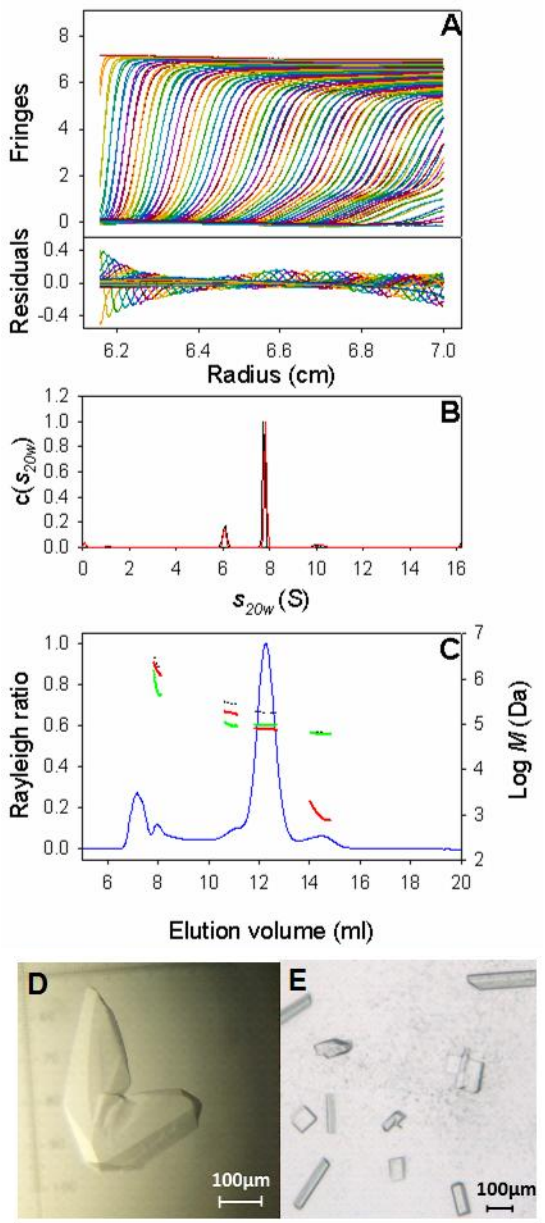

measured in AUC-SV. [b]for FhuA complex in exp. 1, and unresolved LMNG free micelles and FhuA complex in exp. 2-4. [c]from AUC-SV experiments of pure LMNG (Fig 1) for the LMNG concentrations reported on the fourth column.

Fig 4. Characterisation and crystallization of LMNG solubilized FhuA

AUC-SV**: A**: Superposition of experimental and fitted sedimentation velocity profiles (top) and residuals (bottom), obtained at 130 000 g and 4 °C during ≈ 4.5 hours using interference optics and 1.5 mm optical path centerpiece, for 7.5 mg mL^{-1} FhuA solubilized with 12 mM LMNG in 20 mM Tris-HCl pH 8.0, 150 mM NaCl. Reference channel was filled with solvent without LMNG. **B**: Superposition of the normalized $c(s_{20w})$ distributions obtained at 280 nm (red line) and with interference optics (black line). SEC-LS: **C**: Rayleigh ratio measured along the elution profiles, for 35 µL of FhuA at 1 mg mL^{-1} and LMNG at 1.2 mM injected on a Superdex 200 10/300 GL (GE Heathcare) column equilibrated at 6 °C with 100 mM Tris-HCl pH 8.0, 150 mM NaCl, 1 mM EDTA, 0.5 mM LMNG, and molar masses (thick lines, right axis) for the whole complex (black), and LMNG (green) and FhuA (red) contributions, derived from combining light scattering, refractive index, and absorbance at 280 nm detections. **D.** Typical DDAO-solubilized FhuA crystals grown in 0.1 M MES pH 6.0, 10% PEG 6000, 2% DDAO. **E.** Typical LMNG-solubilized FhuA crystals grown in 0.1 M ADA pH 6.5, 12% PEG 6000, 1.2% LMNG.

FhuA crystallization

480 conditions were screened for the crystallization of FhuA solubilized in 1.2% (12 mM) LMNG or, for comparison, 1.6% (79.4 mM) decyldimethylamide-N-oxide (DDAO). DDAO is the detergent in which the protein was historically crystallized [56], and in our hands, FhuA-DDAO crystals diffracting to 2.2 Å could be obtained (Arnaud and Breyton, unpublished data).

The FhuA-LMNG complex is clearly more susceptible to precipitating conditions: only 53.7% of the drops remained clear (*vs*. 86% for FhuA-DDAO). In addition, 13.3% of the conditions with LMNG yielded unambiguous crystal formation *vs*. only 3% in DDAO, and 10 *vs*. 8 conditions, respectively showed single crystals. Whereas conditions allowing single crystal growth in DDAO were closely related (high molar mass PEG, pH 6-7 and $MgCl_2$), those in LMNG displayed more differences: different precipitants, including wide ranges of PEG molar mass (400-8000) and pH (4-9) and a variety of co-crystallization salts. The shapes of the crystals were also very different, with feather-like shapes for FhuA-DDAO and more

rod for FhuA-LMNG crystals (Fig 4D). X-ray diffraction data were collected on FhuA-LMNG crystals (Table 4). Crystals grown in the screening assay, with little optimization, diffracted up to 4 Å, which allowed to get a model at low resolution and to determine the crystal packing. Interestingly, these crystals have a different space groups ($C222_1$) than crystals obtained with DDAO ($P6_1$).

Thus, LMNG largely expanded the number of potential conditions in which FhuA crystals are grown, possibly by allowing different crystal packing. These data seemingly support the idea that LMNG enhances successful crystallization of membrane proteins [26].

Table 4. Characteristics of LMNG solubilized FhuA crystals

Crystal data collection statistics for FhuA – LMNG	
Space group	C 2 2 21
Unit cell dimension (Å)	149.53 210.96 188.7 90 90 90
Number of reflections	371461 (37282)
Number of unique reflections	25522 (2481)
Resolution limits (Å)	40.61 - 4.0
Higher resolution shell (Å)	4.143 - 4.0
Completness	98.13 % (98.06 %)
Redundancy	14.6 (14.8)
Rmerged	0.1771 (7.384)
Rmeasured	0.1838 (7.648)
I/(I)	9.51 (0.50)
Molecular replacement with Phaser	
LLG = 3698.6	
TFZ = 16.4	
Crystallographic refinement statistics	
Resolution range (Å)	40.61 - 4.0
Number of reflections	25098
R / FreeR	0.3141 / 0.3546
Number of atoms (total)	11024
Mean B value ($Å^2$)	209.52
rms deviation from ideal values:	
bond length (Å)	0.007
bond angle (degree)	1.52

SpNOX-LMNG assemblies

We then investigated the prokaryotic enzyme SpNOX [62]. This protein is a recently identified analog to the eukaryotic NOX membrane proteins. They are the central catalytic component, involved in transmembrane electrons transfer, within NADPH oxidase complexes, which play essential roles in *e.g.* immunity, cardiovascular physiology, etc. Despite the progress done in the characterization of the soluble subunits of the NADPH oxidase complexes [83,84], there were very few structural information on the NOX α-helical membranous component up to the recent composite structure of a NOX5 isoform from a cyanobacteria [85]. Apart from its fundamental biological interest, this protein displays several features that make it a convenient model to test and develop new methods or processes in membrane protein biochemistry. Indeed, the red color brought by the presence of two hemes *b* within the transmembrane protein constitutes a good reporter in all steps of

protein manipulation as well as a precious indicator of the correct folding of the protein. Moreover, SpNOX has an enzymatic activity that can be measured spectrophotometrically in a fast and convenient way.

For SpNOX solubilization and purification, maltoside detergents were identified as essential in order to preserve protein activity [62]. However, several lines of improvement have been observed by using LMNG instead of DDM. First, from the elution profile from size exclusion chromatography of the second purification step (Fig 5A), the peak of SpNOX aggregates, at 45 mL, decreases drastically from DDM to LMNG while, in addition to minor amounts of dimers detected in the two conditions, that of monomeric SpNOX, at 70 mL, increases. SpNOX is obtained with an improved homogeneity in LMNG compared to DDM. Moreover, SpNOX shows a significantly increased specific activity in LMNG compared to DDM (Table 5). We evaluate the relative thermal stability of SpNOX in LMNG compared to DDM. T_m in LMNG is drastically increased (+13°C) (Table 2).

Table 5. Compared activities, in LMNG and DDM, of SpNOX and BmrA

Protein	Environment	Activity
SpNOX	DDM 1.27 mM	5.9 +/- 0.5 mol Cyt c reduced s^{-1} mol^{-1} SpNOX
SpNOX	LMNG 0.21 mM	9.3 +/- 0.2 mol Cyt c reduced s^{-1} mol^{-1} SpNOX
BmrA	DDM 2 mM	0.8 +/- 0.1 µmol ATP hydrolyzed min^{-1} mg^{-1} BmrA
BmrA	LMNG 0.1 mM	1.4 +/- 0.2 µmol ATP hydrolyzed min^{-1} mg^{-1} BmrA
BmrA	liposome	5.0 +/- 0.6 µmol ATP hydrolyzed min^{-1} mg^{-1} BmrA

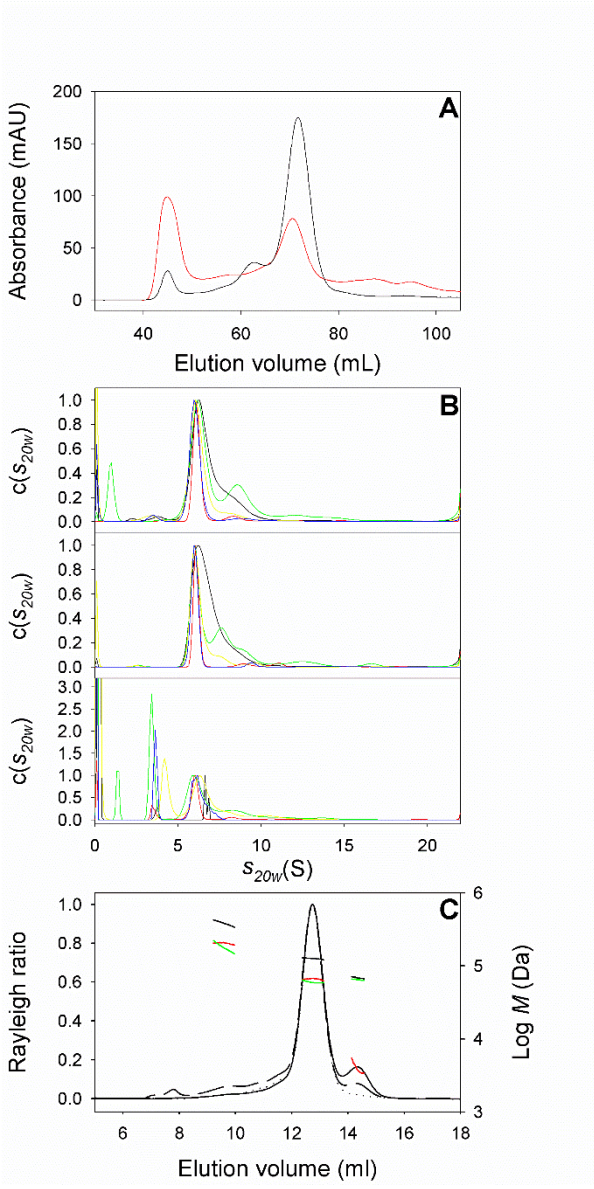

Fig 5. LMNG solubilized SpNOX: preparative SEC, AUC-SV and SEC-LS

A: Superdex 200 16/60 elution profiles, in the second step of SpNOX purification, performed in 50 mM Tris-HCl pH 7, 300 mM NaCl, with either 0.3 mM DDM (red line) or 0.03 mM LMNG (black line). Aggregates elute at 45 mL, while monomeric SpNOX elutes at 70 mL. **B**: Superposition of normalized $c(s_{20w})$ distributions obtained from AUC-SV at 280 nm (top), 412 nm (middle) and with interference optics (bottom), for SpNOX samples *c0.1*, *c3*, *c0.25d*, *c0.1d*, *c0.25dLMNG*, described in the text (black, red, green, yellow, and blue lines, respectively). The vertical dashed line at 6 S indicates the main SpNOX complex **C**: SEC-LS normalized elution profiles obtained at 280 nm (dottled line), by refractive index (continuous line), and light scattering (dashed line), for 30 µL of SpNOX at 2.9 mg mL^{-1} injected on a Superdex 200 10/300 GL (GE Heathcare) column equilibrated at 4 °C with 50 mM Tris-HCl pH 7.0, 300 mM NaCl, 0.05 mM LMNG (buffer A) and molar masses (thick lines, right axis) for the whole complex (black), and LMNG (green) and SpNOX (red) contributions, derived from combining static light scattering, refractive index, and absorbance

at 280 nm detections. A hydrodynamic radius of 4.0 nm was measured by DLS at the maximum of the main peak.

We then investigated, using SV-AUC, homogeneity and association state of SpNOX solubilized in LMNG, at different concentrations of SpNOX and LMNG. After a final SEC purification step with 0.03 mM LMNG in the elution buffer (buffer A, see legend to Fig 5), SpNOX was obtained at 0.1 mg mL^{-1} (sample *c0.1*). Then the protein was concentrated 30 times by ultrafiltration with a 30-kDa cut off membrane (sample *c3*). To further investigate the effects of protein and LMNG concentrations on the size and composition of the LMNG/SpNOX complexes, part of *c3* was rediluted 12 or 30 times in buffer A (containing 0.03 mM LMNG) and 12 times with the same buffer but containing LMNG at 1.5 mM (samples *c0.25d, c0.1d, c0.25dLMNG*, respectively). AUC-SV of these samples was followed at 412 nm, in addition to the usual 280 nm and interference detection, which allows following the heme b cofactors. The normalized $c(s)$ curves (Fig 5B) at 280 and 412 nm superimpose showing that the different SpNOX complexes in all samples have the same heme content. The measured ratio A_{412}/A_{280}=1.75 ± 0.05 is that expected for pure SpNOX [62]. The main SpNOX species (typically 85%) sediments at s_{20w} = 6.0 ± 0.1 S. A minor contribution (typically 8%) is detected at ≈ 8.2 S, in addition to poorly-defined aggregates (typically 7 %). *c0.25dLMNG* appears to be more homogeneous, and *c0.25d* more heterogeneous, but we cannot ascertain the relevance of these subtle variations. We conclude that SpNOX main assemblies have clearly the same composition in all samples, and increasing LMNG or protein concentration does not lead to larger complexes. Interference optics allows the additional detection of LMNG micelles below 4 S, in the expected *s*-range, since we measured *s* at 2.5 and 5 S for pure LMNG at 0.05 and 1.5 mM in buffer A. From the integration of the signal, we derived a concentration of 1.2 mM free micelles in *c3*, which indicated an almost stoechiometrical co-concentration of LMNG and SpNOX. For the main SpNOX complex, the ratio of the interference fringes and A_{280} signals is the same for *c0.1*, *c3*, *c0.25d*, suggesting that no or few LMNG micelles co-sediment (the ratio is however larger for *c0.25dLMNG* and *c0.1d*, but it may be related to the uncertainty of the analysis), and provides a rough estimate of 1 ± 0.1 g g^{-1} LMNG bound to SpNOX (this value is imprecise, as discussed below).

Complementary SEC-LS-DLS in buffer A with 0.05 mM LMNG was performed on four samples of SpNOX from a different purification. One at 0.16 mg mL^{-1} is from SEC, the three others are from subsequent concentration to 1.0, 2.9 and 8.7 mg mL^{-1} (concentration by a factor of 8, 18 and 54, respectively) by ultrafiltration. The elution profiles of the four SpNOX samples are very similar, and one example is shown on Fig 5C. The main SpNOX complex elutes at 12.8 mL with a R_H = 4.0 nm measured from DLS. The analysis provides molar masses for the main complex of 68 ± 3 kDa and 59 ± 3 kDa for SpNOX and LMNG-components, remarkably constant for the four samples. These values correspond to a detergent/protein ratio similar to that estimated from AUC. The protein molar mass, however is intermediate between the theoretical ones for a monomer (48 kDa) and a dimer. This suggests a systematical error in the input value, used in AUC and SEC-LS, of the SpNOX extinction coefficient. We thus rather consider the total molar mass of the complex of 126 kDa, derived from LS and RI detection to derive, in the hypothesis of a monomeric protein,

an amount of bound detergent of 1.6 g/g. Combining *s* from AUC and R_H from DLS, a buoyant molar mass of 26.2 kDa is derived, which corresponds to a globular compact monomer of SpNOX binding 1.6 $g.g^{-1}$ of LMNG, with a frictional ratio of 1.2, corresponding to a globular compact shape.

BmrA-LMNG assemblies

BmrA (for 'Bacillus multidrug resistance ATP') is a member of the ABC ("ATP-Binding Cassette") transporters family. It is capable to export multiple drugs with no chemical relationship [86]. In human, its closest homologue MDR1 confers resistance to chemotherapeutic treatments [63]. Crystal structures of homologs stabilized in different states [87,88] suggest that, to permit drug translocation, large conformational changes must occur in an alternating access model. BmrA could be purified in a functional homodimeric form in 0.05% DDM [89,90], and, indeed it was shown to be flexible and adopt different conformations [91–94].

Since then, the protein was purified in LMNG [95]. It was noticed that LMNG, in contrast to DDM, significantly reduced BmrA aggregation with time. Moreover, the ATPase activity of BmrA was significantly increased, by a factor of about 1.5 to 2, in LMNG compared to DDM (Table 5). The activity in LMNG is thus getting closer to that of the protein reconstituted into liposomes: 1.4 *vs.* 5, respectively, µmol ATP hydrolyzed /min/mg protein (Table 5).

We evaluated by DSF the protein's thermal stability for two freshly purified -in either DDM or LMNG- batches of BmrA. Measurements were done on the Apo and the vanadate (Vi) inhibited forms. The Apo-form is expected to be in an open conformation, the Vi-inhibited form would exist in a closed conformation ([64,93] and unpublished results). Fig 3 shows the measurements for BmrA Apo and Vi-inhibited forms, and Table 2 reports the melting temperatures T_m. In DDM and in LMNG, the T_m increases steadily from the less stable Apo to the more stable Vi-inhibited form. For the two forms, BmrA unfolds at higher temperature when purified in LMNG compared to DDM: by 4.5 °C for BmrA Apo, and ≈ 13 °C for the Vi-inhibited BmrA (Table 2).

Limited proteolysis experiments were performed on the Apo- and Vi-inhibited BmrA forms, to evaluate differences in protein flexibility between the two forms, in DDM and in LMNG. After incubation for different times with a protease, BrmA samples were run on SDS-PAGE. Fig 6A-D show clearly, for BmrA purified in DDM and LMNG, respectively, and incubated with trypsin, the increased robustness of Vi-inhibited BmrA compared to the Apo form. In DDM, the 55 kDa band representing the intact protein essentially disappeared after 30 min of incubation for the Apo form, and more than 300 min for the Vi-inhibited form, in agreement with previously published results [93]. In LMNG, 60 min are required for an almost full disappearance of the intact Apo BmrA, and the Vi-inhibited form is essentially preserved for the entire time period tested. The reduced kinetics of proteolysis in LMNG compared to DDM is also observed with protease V8 (Fig 6E-F). We checked that the detergent type had no effect on protease activity by itself.

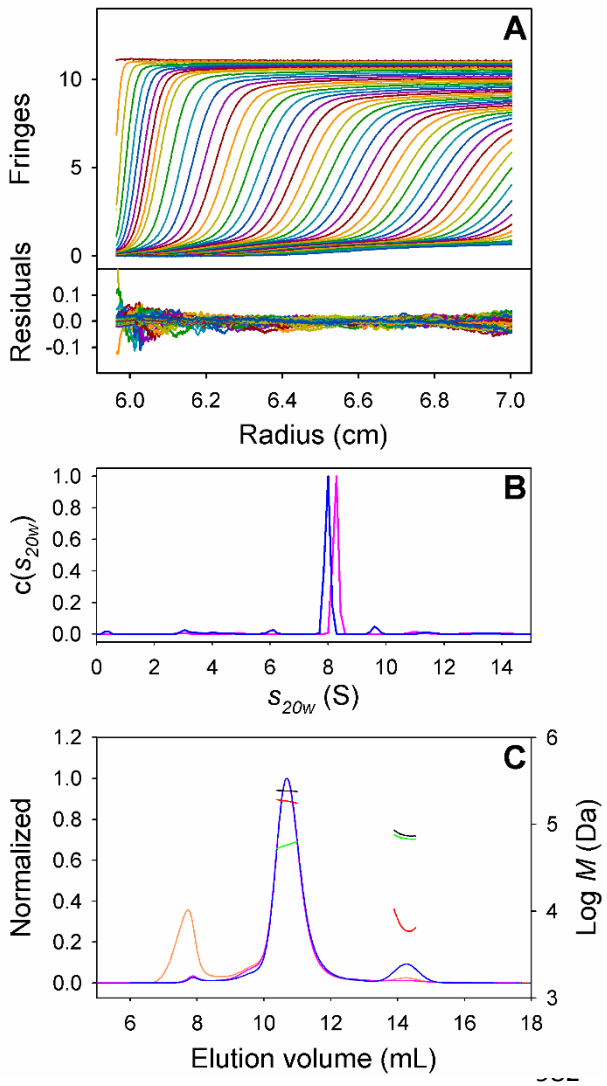

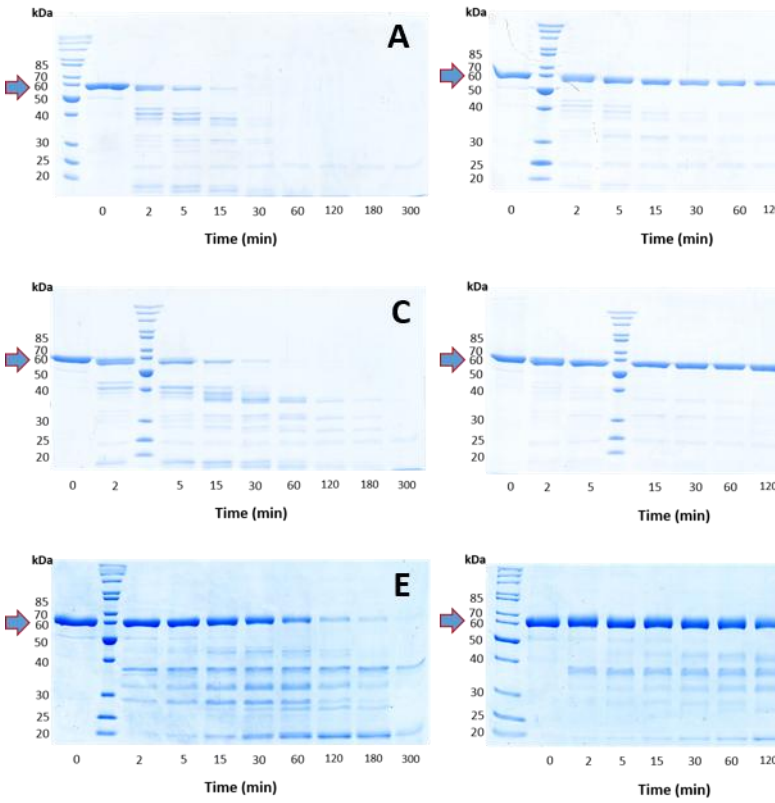

Fig 6. BmrA limited proteolysis experiments
A-D: incubation with trypsin at 1 µg/250 µg of protein, for **A**: Apo BmrA in DDM, **B**: Vi-inhibited BmrA in DDM, **C**: Apo BmrA in LMNG, **D**: Vi-inhibited BmrA in LMNG. **E-F**: incubation with protease V8 at 1 µg/20 µg of protein, for Apo BmrA, in **E**: DDM, and **F**: LMNG. DDM and LMNG concentrations are 2 and 0.1 mM, respectively. Time zero is taken after 15 min of pre-incubation before adding the proteases. The arrows indicate intact BmrA.

In order to evaluate protein homogeneity in LMNG, samples of BmrA were purified with a last step of SEC in a buffer containing LMNG at 0.1 mM, concentrated using a centrifugal filter device by a factor of 4.4 for a final BmrA concentration of 1.3 mg mL^{-1}. SV-AUC revealed a very homogeneous preparation, with one protein complex at s_{20w} = 8.2 S (experimental value of 4.2S, at 10 °C, in the buffer containing glycerol) (Fig 7A). SEC-LS experiments, done with a BmrA sample at 2.7 mg mL^{-1}, prepared in a similar way, stored frozen at -80 °C and injected on a column equilibrated with buffer A, showed minor (total ≈ 5%) contributions of large and small aggregates eluting at 7.8 mL and as a shoulder at 9.7 mL, in addition to the main complex, eluting at 10.7 mL, with a R_H = 5.5 nm measured from DLS, and a total molar mass of 240 kDa, corresponding to a dimer with 0.8 g/g bound detergent (Fig 7B). Combining R_H and the *s*-values, we derived a buoyant molar mass of 45.9 kDa, corresponding to a dimer with 0.6 g/g bound LMNG, and a frictional ratio of 1.35. Excess LMNG micelles were undetected in the AUC experiments; in SEC-LS their amount corresponds to an injected LMNG concentration of 0.2 mM. In conclusion, very homogeneous BmrA samples can be prepared in LMNG with protein concentration in the mg mL^{-1} range, which remains essentially homogeneous after storage at -80 °C.

Fig 7. LMNG solubilized BmrA in AUC-SV and SEC-MALS

AUC-SV**:** **A**: Superposition of experimental and fitted sedimentation velocity profiles (top) and residuals (bottom), obtained at 130,000 g and 10 °C during ≈ 8 hours using interference optics and 12 mm optical path centerpiece, for BmrA at 2.3 mg mL^{-1} and free LMNG at 0.44 mM (putative concentration) in 25 mM Tris-HCl pH 8.0, 150 mM NaCl, 10% glycerol. Reference channel was filled with solvent without LMNG. **B**: Superposition of the normalized $c(s_{20w})$ distributions obtained at 280 nm (pink line) and with interference optics (blue line). SEC-LS: **C**: Rayleigh ratio, refractive index, and absorbance at 280 nm (orange, blue, and pink lines, respectively) measured along the elution profiles, for 50 µL of BmrA at 2.7 mg mL^{-1} and free LMNG at 0.06 mM, this concentration being experimentally determined in SEC-LS, injected on a Superdex 200 10/300 GL (GE Heathcare) column equilibrated at 4 °C with 50 mM Tris-HCl pH 7.0, 300 mM NaCl, 0.05 mM LMNG (buffer A), and molar masses (thick lines, right axis) for the whole complex (black), and LMNG (green) and BmrA (red) contributions, derived from combining the three detections. The protein elutes as a main species at 10.7 mL, together with large and small aggregates, in minor amounts, in the void volume (7.8 mL) and as a shoulder at 9.7 mL, respectively; free LMNG elutes at 14.2 mL.

bR homogeneity, and time and thermal stability

Lastly, we investigated the homogeneity and time stability of the bR as a model protein. bR is a light-driven proton pump purified from the archaea *Halobacterium*. It is composed of seven transmembrane α-helices and binds a covalent cofactor, a retinal molecule that confers purple color to the protein.

Sucrose gradients are a convenient means to perform both detergent exchange and evaluate the colloidal homogeneity of the protein-detergent complex. In the case of colored proteins, this latter information is directly visible after centrifugation, by the broadness of the protein-detergent band. We routinely use this method to evaluate the potentialities of fluorinated surfactants in the biochemistry of membrane proteins, using the bR. Fig 8A shows the results of sucrose density gradient experiments in the presence of 1 mM DDM, or 0.2, 2 and 20 mM LMNG. After 15 h centrifugation, the protein migrated past the middle of the gradient, insuring total detergent exchange, as checked by TLC. In all LMNG conditions, the protein band migrates at the same depth and appears to have the same width/broadness as that in DDM, suggesting that the bR-LMNG complexes are homogeneous monomers as the bR-DDM complexes. The retinal molecule, whose visible absorption spectrum is very sensitive to its local environment, is a convenient reporter of the state of the protein: the trimeric protein in its native membrane reveals a visible absorption spectrum with a maximum at λ_{max} = 570 nm; when solubilized in detergent, the protein monomerises and displays λ_{max} = 554 nm; in both cases, the protein appears purple. When the protein denatures, the retinal is released, and λ_{max} shifts to 400–380 nm: the protein solution turns yellow. Fig 8B and 8C report the absorption spectra of the protein recovered just after centrifugation and three months after, stored on ice in the dark. The DDM sample, which appears pinkish in the gradient, displays a broad absorption peak, with a λ_{max} ~ 530 nm (Fig 8B), suggesting a poorly folded protein. After three months however, the spectrum shows a usual peak, with λ_{max} = 555 nm. The protein probably started to denature in OTG, the detergent used for its solubilization, but returned to its native fold when transferred to DDM. In all LMNG samples, the absorption peak displays a λ_{max} = 554 nm (Fig 8C), suggesting that the dynamics of the bR monomer in LMNG is different than in classical detergents. After three months incubation, the absorption spectra are unchanged, indicating that the protein is very stable.

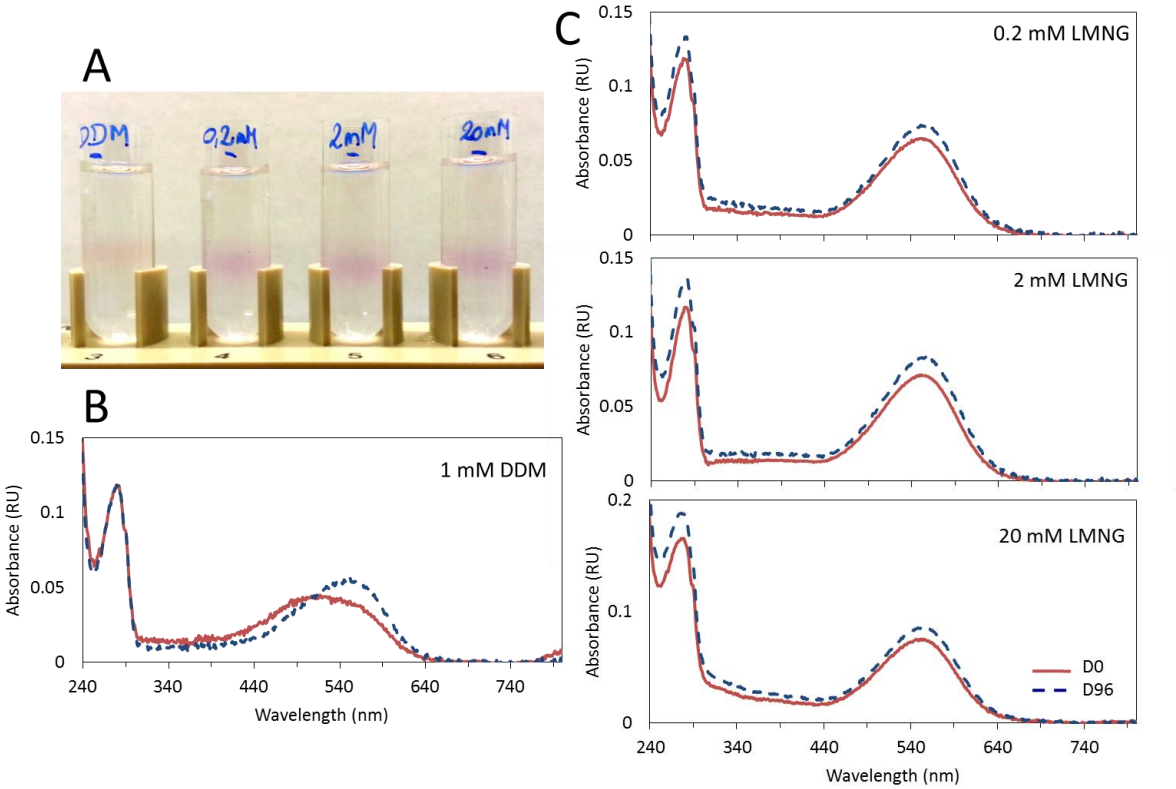

Fig 8. bR sucrose gradient

A: Migration of bR in 10-30% sucrose gradients in the presence of either 1 mM DDM, 0.2, 2 or 20 mM LMNG. Gradients were centrifuged 15 h at 200,000 x *g*. bR was recovered from the gradients and its UV-visible spectrum measured immediately (D0, solid line) or three months after incubation at 4°C in the dark (D96, dashed line). **B**: bR in 1 mM DDM, **C**: bR in 0.2, 2 and 20 mM LMNG.

At last, bR thermal denaturation assays were performed. Solubilized bR samples were incubated with biobeads to decrease the OTG concentration, and diluted 18 times (leading to a residual OTG concentration of 0.4 times the CMC) in OTG, DDM, or LMNG, at a concentration of 2 mM above the CMC of each detergent, for thermal denaturation assays. Result are presented on Fig 3 and Table 2. bR has an increased thermostability in DDM compared to OTG, and LMNG is even more stabilizing, with T_m increased by 6 and 12 °C, respectively.

Discussion and conclusion

On the self-assembly of LMNG

From AUC experiments, we determined the CMC of LMNG to be 40 µM. This is coherent with previously published value from from hydrophobic dye solubilization measurements (10 µM) [26], while isothermal titration calorimetry measurements yielded a significantly lower concentration (11.3 nM) [44]. The CMC is not an absolute value, rather a range of concentrations, and different techniques used to determine the CMC probe different properties of micelle formation. Thus, it is not unusual to find different values depending on the technique used, and discrepancies become exacerbated when the CMC is very low.

Regarding the size of the micelles, the s_{20w}-value of LMNG at 0.25 mM (0.025 %) is 3.3 S. This value is in the same range than that of DDM (3.12 S) that forms globular compact

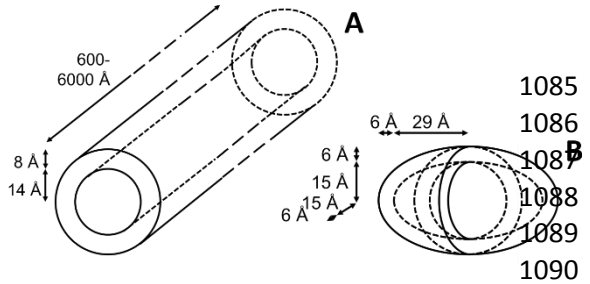

micelles of about 60 kDa in a large range of detergent concentration [65]. If LMNG forms quite small micelles at 0.25 mM, AUC, DLS, SAXS, and SANS, clearly indicate it forms larger micelles, rods of increasing length, when increasing the concentration above 0.25 mM. The lateral dimension of the hydrophobic core radius is 14 Å, and that of the shell thickness is 7 Å in H_2O (9 Å in D_2O). These values correspond to that of DDM micelles, described from SAXS to form oblate ellipsoids with, in the minor axis, a hydrophobic core of ≈ 15 Å surrounded by a hydrophilic layer of ≈ 6 Å thickness [96,97] (Scheme 2). The differences of 1 Å between our LMNG and the published DDM dimensions are not significant since different techniques and buffers, thus contrasts (in terms of electron density or neutron scattering length densities), were used. To this date, this is only one membrane protein pdb file (4b4a) containing LMNG as a ligand (pdf identifier "LMN"). The maximum C-O, C-C and O-O distances in the whole molecule, in the two tails, and in the two heads, respectively, are 21.9, 13 and 11, 9.8 and 9.7 Å, respectively (we note that in this unique structure, the hydrophilic head is quite open: we measure a maximal distance between the O of the two sugars of LMNG of 19 Å). For DDM as a ligand (pdf identifier "LMT"), in an arbitrary selection of membrane protein pdb files (6haw, 6hqb, 4kfm, 6cnn), we measure maximal distances for the whole molecule, the tail, and the head, of 20.5 +/- 1, 12 +/- 1, and 9.2 +/- 0.8 Å, respectively. These values are logically similar to that of LMNG. The maximum length of the tail is logically lower than 16.7 Å corresponding to the dimension of an extended alkyl chain with 12 carbons [97].

If DDM is described to form slightly elongated micelles, for LMNG at 20 mM however, we measured lengths of 600 Å in H_2O and more than 5000 Å in D_2O. It corresponds to LMNG rods with ratios of the total length over the total diameter, of 14 and 120. For LMNG in H_2O, the rod length value coincides with the maximum distances estimated between 10 and 20 mM LMNG, from the pair distribution analysis of the – measured independently – SAXS data of Fig 2A. In a preliminary independent SANS experiment, however, rods of only 1200 Å long were modelled for LMNG micelles at 20 mM in D_2O. It corresponds to a length over diameter ratio of 28, 4-5 times smaller than that presented above. It is likely that the precise length of LMNG rods depends on uncontrolled parameters during sample preparation. It is possible that LMNG forms longer rods in D_2O, compared to H_2O, but we cannot ascertain it. For both SAXS and SANS, the shape and size of the micelles does not change between 10 and 20 mM.

Scheme 2. Schematic representation of LMNG and DDM micelles

A: LMNG micelles at 20 mM in H_2O or D_2O, from modelling of combined SANS and SAXS data (this work) **B**: DDM micelles from modelling of SAXS data [96,97].

Israelachvili et al. [98,99] have provided a rational to explain how the molecular geometry of individual surfactant molecules affects and controls the shape and size of the assemblies they form. The geometry of the molecule can be described by three parameters: the area of the hydrated polar head, a_0, the volume, v, and the extension, l_c, of the hydrophobic tail. The

value of the related critical packing parameter, $v/(a_0 l_c)$, representing the ratio of the mean area of the hydrophobic tail on that of the hydrophilic head, determines the geometry of the assemblies: for $v/(a_0 l_c) < 1/3$ (large hydrophilic surface), spherical micelles are formed; for $1/3 < v/(a_0 l_c) < 1/2$, rods are favored; then, for $v/(a_0 l_c) < 1$, ~ 1, and > 1 (with increasingly large hydrophobic lateral extensions), flexible or planar bilayers, and inverted micelles, respectively, are stabilized. The LMNG molecule corresponds to two linked DDM molecules. The linkage is done through a quaternary carbon, localized on the lauryl chain, at the second carbon following the ether group belonging to the maltose moiety. It is thus at the junction between the hydrophilic head and the hydrophobic tail of the detergent. The constraints of this link on each moiety dimensions are hardly intuitively predictable. The fact that DDM forms globular micelle while LMNG forms rod means that the packing parameter $v/(a_0 l_c)$ increases from DDM to LMNG, which can be related to an increase, in LMNG compared to DDM of the hydrophilic surface per maltose group, and/or of the mean length of the hydrophobic chain, corresponding to changes in their landscape of the molecular conformational stability and/or dynamics.

Rod formation has noticeable consequences for biochemists. When using ultrafiltration centrifugal devices to concentrate proteins, LMNG co-concentrates with the membrane protein by the same factor. Depending on the initial detergent concentration, typically from 0.02 to 0.1 mM, LMNG in the concentrated sample will form small to very large assemblies. Concentrated LMNG dissociates upon SEC, but elutes as a very broad peak, preventing membrane protein in concentrated LMNG to be recovered with a well-defined LMNG concentration.

On the relative stabilization of proteins in LMNG compared to DDM

Our work corroborates the stabilizing propensity of LMNG towards membrane proteins, already described in the literature (see the introduction). All four proteins investigated here are thermally stabilized in LMNG compared to DDM. The temperature shift is very large, both for FhuA (+11 °C), a very stable β-barrel protein, and for SpNOX (+13 °C), a fragile α-helical protein. For the flexible BmrA, temperature shifts between 4 and 13 °C are observed depending on the presence or absence of ligands. For bR, the gain is 6 °C. SpNOX solubilized and partially purified in LMNG shows a significantly decreased content of aggregates, corresponding to an increased stability. The reduced kinetics of limited proteolysis in LMNG compared to DDM for the Apo and the Vi-inhibited forms of BmrA, expected to represent the open and closed conformations, could have suggested some restricted flexibility of the protein. However, the protein is more active in LMNG as compared to DDM thereby indicating that the flexibility required for ATPase activity is not impaired in LMNG. Indeed, in LMNG, BmrA seems to be more prone to reach or stabilize the closed conformation which is required to get a high ATPase activity. Hence, BmrA is in a more stable and perhaps, more physiologically relevant conformations in LMNG as compared to DDM. Restricted protein flexibility is also suggested for bR, which UV-visible spectrum displays a maximum absorption peak close to that of the constrained trimer in the purple membrane, far from that of the more flexible monomer in DDM. These results are in the line with the restraint of protein inter-conversion dynamics measured for GPCRs. The reduced dynamics of proteins may be related to the strong binding of the LMNG correlated to its low CMC, deriving from the connection of the two hydrophobic tails in its structure. As for BmrA, SpNOX displays an increased specific activity in LMNG compared to DDM, which may reflect a significantly higher proportion of inactive protein in DDM compared to LMNG, or be related to a difference in SpNOX flexibility, or to the stabilization of some conformations.

On the assembly of LMNG-membrane proteins

The solubilized membrane proteins investigated in this work have the same quaternary structure in LMNG as in their usual detergent: FhuA, SpNOX, and bR, are monomeric and BmrA is dimeric. In the case of SpNOX, dimers of the main species –probably inactivated forms– are detected in LMNG, for typically 10%, the proportion varying slightly depending on the purification. These species are also detected in DDM. In the AUC experiments where LMNG concentration was voluntarily raised to 24 mM, FhuA and SpNOX association states were not affected. The amount of bound detergent did not vary too, despite rod micelles of LMNG are expected at these large concentrations. This behavior was not anticipated. We previously investigated fluorinated surfactants (for reviews, see [8,16,17]), and, in a series of surfactants whose polar head size was modulated by the presence of one, two, or three glucose moieties, homogeneous complexes with bR and cytochrome b_6f were obtained only with the compounds that form homogeneous micelles, *i.e.* the surfactants with the more voluminous head. In the surfactant forming long rods, with only one glucose, the membrane proteins were soluble and active, but formed heterogeneous detergent protein complexes. We anticipated it could be related to the heterogeneity in the amount of bound detergent [100]. Other fluorinated surfactants with relatively small head groups (lactoside, maltoside, octaethylene glycol ether) formed large and polydisperse, probably rod-like assemblies, and indeed formed also large and heterogeneous complexes with membrane proteins (refs in [100]). By contrast, the fluorinated surfactant F-TAC (now commercialized by Calixar), which has a voluminous polymeric hydrophilic head, was shown to assemble into small micelles and form well defined complexes with membrane proteins. The present work on LMNG shows that large size of surfactant micelle does not necessarily translate into protein detergent complex heterogeneity.

On the assembly of LMNG-membrane proteins: bound detergent

In the case of FhuA, previous measurements determined 1.2 g of bound DDM per g of protein, using SEC in the presence of radiolabeled DDM [81]. This value is close to 1 and 1.2 g g^{-1} determined in the present work for the protein solubilized in LMNG by AUC and SEC-LS. For BmrA, the amount of bound LMNG (0.6 g g^{-1}) we determined by combining *s*- and R_H-values, is lower but in the same order of magnitude than that determined for bound DDM by the same technique (0.9 g g^{-1})[101]. A similar trend, in the comparison of DDM and LMNG bound to BmrA, was reported using MALDI/TOF for the evaluation of bound detergent [7]. These estimates of bound DDM to BmrA are much lower than that determined by SEC in the presence of radiolabeled DDM (1.5 g g^{-1})[89], which emphasizes the difficulty to determine precisely bound detergent. Nevertheless, these comparisons presented in Table 6, show that the amounts of bound detergent are similar whether the protein is solubilized in DDM or LMNG. It means that the amount in mol/mol is nearly twice for DDM than for LMNG, and it is possible that the amount (in g g^{-1}) of bound LMNG is slightly less compared to that of DDM.

Table 6. Bound LMNG and DDM to FhuA, BmrA, and SpNOX

Protein	detergent	Bound detergent		technique	reference
		g/g	mol/mol*		
FhuA	DDM	1.2	188	SEC/[^{14}C]DDM	[81]
FhuA	LMNG	1.0	80	AUC	present work
FhuA	LMNG	1.2	95	SEC-LS	[81]

BmrA	DDM	0.9	234	AUC+ SEC-LS	[101]
BmrA	DDM	1.3-1.6	388-416	MALDI/TOF	[7]
BmrA	DDM	1.5	390	SEC/[^{14}C]DDM	[89]
BmrA	LMNG	0.6	79	AUC+ SEC-LS	present work
BmrA	LMNG	1.1-1.3	145-171	MALDI/TOF	[7]
SpNOX	LMNG	1.6	77	AUC+ SEC-LS	present work

* considering FhuA and SpNOX as monomers, and BmrA as a dimer.

On the crystallization of LMNG-membrane protein

The high resolution structures of several GPCRs were obtained thanks to purification in LMNG (cf Introduction) followed by crystallization in mesophase, a process in which the membrane protein in the crystal is stripped off from its bound detergent [102]. Crystallization in LMNG using vapor diffusion was described for *e.g.* the cytochrome b_6f complex [26], the TatC core of the twin-arginine protein transporter [50], an ABC transporter lipid-linked oligosaccharide flippase [41], a borate efflux transporter [51], and a plant voltage-gated two-pore channel [52]. FhuA is yet another one. One of our motivations, in crystallizing this well described protein, was to check whether the ability to obtain crystals was prevented by the presence of large LMNG assemblies in the membrane protein sample. It is clearly not the case, and on the contrary, comparing the behavior of the protein in crystallization screens, we observed that the number of initial hits was larger when the protein was solubilized in LMNG when compared to the classically used DDAO. The space group of crystals of FhuA grown in LMNG is not the same as that of the protein grown in DDAO. However, this is not remarkable, as the same space group is found when the protein is crystallized in LDAO.

To summarize, the interest of structural biologists for LMNG is very strong, since it stabilizes noticeably most membrane proteins compared to other detergents. Due to its low desorption kinetics, it would stabilize membrane proteins even in sub-CMC concentrations. It forms large rod assemblies at concentration above the sub mM range, but, for the examples we investigated, the solubilized proteins remain as homogeneous as in usual detergents, with similar amounts of bound detergent, and the presence of the large LMNG micelles does not prohibit membrane protein crystallization using vapor diffusion or mesophase.

Acknowledgment

This work used the platforms of the Grenoble Instruct centre (ISBG; UMS 3518 CNRS-CEA-UJF-EMBL) with support from FRISBI (ANR-10-INSB-05-02) and GRAL (ANR-10-LABX-49-01) within the Grenoble Partnership for Structural Biology (PSB). Gina Reyes-Mejia, Marie-Ange Marrel, Séraphine Crassac, and Emma Lundell (UGA) performed BmrA and FhuA preparations, FhuA and bR thermal denaturation assays, respectively, during their master internships at IBS; Marie-Pierre Candusso for advices with BmrA limited proteolysis; Adam Round and Martha Brennich (ESRF), and Frank Gabel (IBS), for help in SAXS data acquisistion. This work benefited from the use of the SasView application, originally developed under NSF Award DMR-0520547. SasView also contains code developed with funding from the EU Horizon 2020 programme under the SINE2020 project Grant No 654000. This work was supported by the French Agence Nationale de la Recherche (ANR-16-CE92-0001) to CE and CB, (ANR-14-CE09-0024B) to JMJ and (ANR-17-CE11-0013) to JD, CH, FF, AV, IPH, MT. A. Vermot thanks for her support through the Emergence program from the Univ. Grenoble Alpes.

References :

[1] M. le Maire, P. Champeil, J.V. Moller, Interaction of membrane proteins and lipids with solubilizing detergents, Biochim Biophys Acta. 1508 (2000) 86–111.

[2] J.-L. Popot, Extracting Membrane Proteins from Their Native Environment, in: Membr. Proteins Aqueous Solut. Deterg. Amphipols, Springer International Publishing, 2018: pp. 59–95.

[3] C. Breyton, C. Tribet, J. Olive, J.-P. Dubacq, J.-L. Popot, Dimer to monomer conversion of the cytochrome b6f complex. Causes and consequences, J Biol Chem. 272 (1997) 21892–900.

[4] S. Lee, A. Mao, S. Bhattacharya, N. Robertson, R. Grisshammer, C.G. Tate, N. Vaidehi, How Do Short Chain Nonionic Detergents Destabilize G-Protein-Coupled Receptors?, J. Am. Chem. Soc. 138 (2016) 15425–15433. doi:10.1021/jacs.6b08742.

[5] C. Chipot, F. Dehez, J.R. Schnell, N. Zitzmann, E. Pebay-Peyroula, L.J. Catoire, B. Miroux, E.R.S. Kunji, G. Veglia, T.A. Cross, P. Schanda, Perturbations of Native Membrane Protein Structure in Alkyl Phosphocholine Detergents: A Critical Assessment of NMR and Biophysical Studies, Chem. Rev. 118 (2018) 3559–3607. doi:10.1021/acs.chemrev.7b00570.

[6] Q. Zhang, H. Tao, W.-X. Hong, New amphiphiles for membrane protein structural biology, Methods San Diego Calif. 55 (2011) 318–323. doi:10.1016/j.ymeth.2011.09.015.

[7] V. Chaptal, F. Delolme, A. Kilburg, S. Magnard, C. Montigny, M. Picard, C. Prier, L. Monticelli, O. Bornert, M. Agez, S. Ravaud, C. Orelle, R. Wagner, A. Jawhari, I. Broutin, E. Pebay-Peyroula, J.-M. Jault, H.R. Kaback, M. le Maire, P. Falson, Quantification of Detergents Complexed with Membrane Proteins, Sci. Rep. 7 (2017) 41751. doi:10.1038/srep41751.

[8] G. Durand, M. Abla, C. Ebel, C. Breyton, New amphiphiles to handle membrane proteins: "ménage à trois" between chemistry, physical-chemistry and biochemistry, in: Membr. Proteins Prod. Struct. Anal., Springer, I. Muss-Veteau, 2014.

[9] J.-L. Popot, Alternatives to Detergents for Handling Membrane Proteins in Aqueous Solutions, in: Membr. Proteins Aqueous Solut. Deterg. Amphipols, Springer International Publishing, 2018: pp. 97–149.

[10] C.E. Schafmeister, L.J.W. Miercke, R.A. Stroud, Structure at 2.5 Å of a designed peptide that maintains solubility of membrane proteins, Science. 262 (1993) 734–738.

[11] X. Zhao, Y. Nagai, P.J. Reeves, P. Kiley, H.G. Khorana, S. Zhang, Designer short peptide surfactants stabilize G protein-coupled receptor bovine rhodopsin, Proc. Natl. Acad. Sci. U. S. A. 103 (2006) 17707–17712. doi:10.1073/pnas.0607167103.

[12] K. Corin, P. Baaske, D.B. Ravel, J. Song, E. Brown, X. Wang, C.J. Wienken, M. Jerabek-Willemsen, S. Duhr, Y. Luo, D. Braun, S. Zhang, Designer lipid-like peptides: a class of detergents for studying functional olfactory receptors using commercial cell-free systems, PloS One. 6 (2011) e25067. doi:10.1371/journal.pone.0025067.

[13] H. Tao, S.C. Lee, A. Moeller, R.S. Roy, F.Y. Siu, J. Zimmermann, R.C. Stevens, C.S. Potter, B. Carragher, Q. Zhang, Engineered nanostructured β-sheet peptides protect membrane proteins, Nat. Methods. 10 (2013) 759–761. doi:10.1038/nmeth.2533.

[14] C. Tribet, R. Audebert, J.-L. Popot, Amphipols : polymers that keep membrane proteins soluble in detergent-free aqueous solutions, Proc Nat Acad Sci USA. 93 (1996) 15047–15050.

[15] J.-L. Popot, Membrane Proteins in Aqueous Solutions: From Detergents to Amphipols, Springer International Publishing, 2018. //www.springer.com/de/book/9783319731469 (accessed June

13, 2018).

[16] C. Breyton, B. Pucci, J.-L. Popot, Amphipols and fluorinated surfactants: Two alternatives to detergents for studying membrane proteins in vitro, Methods Mol. Biol. 601 (2010) 219–245. doi:10.1007/978-1-60761-344-2_14.

[17] J.-L. Popot, Amphipols, nanodiscs, and fluorinated surfactants: three nonconventional approaches to studying membrane proteins in aqueous solutions, Annu. Rev. Biochem. 79 (2010) 737–775. doi:10.1146/annurev.biochem.052208.114057.

[18] R. Matar-Merheb, M. Rhimi, A. Leydier, F. Huché, C. Galián, E. Desuzinges-Mandon, D. Ficheux, D. Flot, N. Aghajari, R. Kahn, A. Di Pietro, J.-M. Jault, A.W. Coleman, P. Falson, Structuring detergents for extracting and stabilizing functional membrane proteins, PloS One. 6 (2011) e18036. doi:10.1371/journal.pone.0018036.

[19] P.S. Chae, P.D. Laible, S.H. Gellman, Tripod Amphiphiles for Membrane Protein Manipulation, Mol. Biosyst. 6 (2010) 89–94.

[20] P.S. Chae, K.H. Cho, M.J. Wander, H.E. Bae, S.H. Gellman, P.D. Laible, Hydrophobic variants of ganglio-tripod amphiphiles for membrane protein manipulation, Biochim. Biophys. Acta. 1838 (2014) 278–286. doi:10.1016/j.bbamem.2013.09.011.

[21] Q. Zhang, X. Ma, A. Ward, W.-X. Hong, V.-P. Jaakola, R.C. Stevens, M.G. Finn, G. Chang, Designing facial amphiphiles for the stabilization of integral membrane proteins, Angew. Chem. Int. Ed Engl. 46 (2007) 7023–7025. doi:10.1002/anie.200701556.

[22] P.S. Chae, K. Gotfryd, J. Pacyna, L.J.W. Miercke, S.G.F. Rasmussen, R.A. Robbins, R.R. Rana, C.J. Loland, B. Kobilka, R. Stroud, B. Byrne, U. Gether, S.H. Gellman, Tandem facial amphiphiles for membrane protein stabilization, J. Am. Chem. Soc. 132 (2010) 16750–16752. doi:10.1021/ja1072959.

[23] S.C. Lee, B.C. Bennett, W.-X. Hong, Y. Fu, K.A. Baker, J. Marcoux, C.V. Robinson, A.B. Ward, J.R. Halpert, R.C. Stevens, C.D. Stout, M.J. Yeager, Q. Zhang, Steroid-based facial amphiphiles for stabilization and crystallization of membrane proteins, Proc. Natl. Acad. Sci. U. S. A. 110 (2013) E1203-1211. doi:10.1073/pnas.1221442110.

[24] P.S. Chae, S.G.F. Rasmussen, R.R. Rana, K. Gotfryd, A.C. Kruse, A. Manglik, K.H. Cho, S. Nurva, U. Gether, L. Guan, C.J. Loland, B. Byrne, B.K. Kobilka, S.H. Gellman, A new class of amphiphiles bearing rigid hydrophobic groups for solubilization and stabilization of membrane proteins, Chem. Weinh. Bergstr. Ger. 18 (2012) 9485–9490. doi:10.1002/chem.201200069.

[25] P.S. Chae, R.R. Rana, K. Gotfryd, S.G.F. Rasmussen, A.C. Kruse, K.H. Cho, S. Capaldi, E. Carlsson, B. Kobilka, C.J. Loland, U. Gether, S. Banerjee, B. Byrne, J.K. Lee, S.H. Gellman, Glucose-neopentyl glycol (GNG) amphiphiles for membrane protein study, Chem. Commun. Camb. Engl. 49 (2013) 2287–2289. doi:10.1039/c2cc36844g.

[26] P.S. Chae, S.G.F. Rasmussen, R.R. Rana, K. Gotfryd, R. Chandra, M.A. Goren, A.C. Kruse, S. Nurva, C.J. Loland, Y. Pierre, D. Drew, J.-L. Popot, D. Picot, B.G. Fox, L. Guan, U. Gether, B. Byrne, B. Kobilka, S.H. Gellman, Maltose-neopentyl glycol (MNG) amphiphiles for solubilization, stabilization and crystallization of membrane proteins, Nat. Methods. 7 (2010) 1003–1008. doi:10.1038/nmeth.1526.

[27] A. Sadaf, J.S. Mortensen, S. Capaldi, E. Tikhonova, P. Hariharan, O. de Castro Ribeiro, C.J. Loland, L. Guan, B. Byrne, P.S. Chae, A Class of Rigid Linker-bearing Glucosides for Membrane Protein Structural Study, Chem. Sci. 7 (2016) 1933–1939. doi:10.1039/C5SC02900G.

[28] M. Ehsan, Y. Du, N.J. Scull, E. Tikhonova, J. Tarrasch, J.S. Mortensen, C.J. Loland, G.

Skiniotis, L. Guan, B. Byrne, B.K. Kobilka, P.S. Chae, Highly Branched Pentasaccharide-Bearing Amphiphiles for Membrane Protein Studies, J. Am. Chem. Soc. 138 (2016) 3789–3796. doi:10.1021/jacs.5b13233.

[29] H. Hussain, J.S. Mortensen, Y. Du, C. Santillan, O. Ribeiro, J. Go, P. Hariharan, C.J. Loland, L. Guan, B.K. Kobilka, B. Byrne, P.S. Chae, Tandem malonate-based glucosides (TMGs) for membrane protein structural studies, Sci. Rep. 7 (2017) 3963. doi:10.1038/s41598-017-03809-3.

[30] K.H. Cho, O. Ribeiro, Y. Du, E. Tikhonova, J.S. Mortensen, K. Markham, P. Hariharan, C.J. Loland, L. Guan, B.K. Kobilka, B. Byrne, P.S. Chae, Mesitylene-Cored Glucoside Amphiphiles (MGAs) for Membrane Protein Studies: Importance of Alkyl Chain Density in Detergent Efficacy, Chem. Weinh. Bergstr. Ger. 22 (2016) 18833–18839. doi:10.1002/chem.201603338.

[31] M. Das, Y. Du, J.S. Mortensen, O. Ribeiro, P. Hariharan, L. Guan, C.J. Loland, B.K. Kobilka, B. Byrne, P.S. Chae, Butane-1,2,3,4-tetraol-based amphiphilic stereoisomers for membrane protein study: importance of chirality in the linker region, Chem. Sci. 8 (2017) 1169–1177. doi:10.1039/c6sc02981g.

[32] P.S. Chae, M.J. Wander, K.H. Cho, P.D. Laible, S.H. Gellman, Carbohydrate-containing Triton X-100 analogues for membrane protein solubilization and stabilization, Mol. Biosyst. 9 (2013) 626–629. doi:10.1039/c3mb25584k.

[33] P.S. Chae, H.E. Bae, M. Das, Adamantane-based amphiphiles (ADAs) for membrane protein study: importance of a detergent hydrophobic group in membrane protein solubilisation, Chem. Commun. Camb. Engl. 50 (2014) 12300–12303. doi:10.1039/c4cc05746e.

[34] S.G.F. Rasmussen, H.-J. Choi, J.J. Fung, E. Pardon, P. Casarosa, P.S. Chae, B.T. Devree, D.M. Rosenbaum, F.S. Thian, T.S. Kobilka, A. Schnapp, I. Konetzki, R.K. Sunahara, S.H. Gellman, A. Pautsch, J. Steyaert, W.I. Weis, B.K. Kobilka, Structure of a nanobody-stabilized active state of the β(2) adrenoceptor, Nature. 469 (2011) 175–180. doi:10.1038/nature09648.

[35] D.M. Rosenbaum, C. Zhang, J.A. Lyons, R. Holl, D. Aragao, D.H. Arlow, S.G.F. Rasmussen, H.-J. Choi, B.T. Devree, R.K. Sunahara, P.S. Chae, S.H. Gellman, R.O. Dror, D.E. Shaw, W.I. Weis, M. Caffrey, P. Gmeiner, B.K. Kobilka, Structure and function of an irreversible agonist-β(2) adrenoceptor complex, Nature. 469 (2011) 236–240. doi:10.1038/nature09665.

[36] T.T. Selao, R. Branca, P.S. Chae, J. Lehtiö, S.H. Gellman, S.G.F. Rasmussen, S. Nordlund, A. Norén, Identification of chromatophore membrane protein complexes formed under different nitrogen availability conditions in Rhodospirillum rubrum, J. Proteome Res. 10 (2011) 2703–2714. doi:10.1021/pr100838x.

[37] X. Jiang, L. Guan, Y. Zhou, W.-X. Hong, Q. Zhang, H.R. Kaback, Evidence for an intermediate conformational state of LacY, Proc. Natl. Acad. Sci. U. S. A. 109 (2012) E698-704. doi:10.1073/pnas.1201107109.

[38] A. Amin, P. Hariharan, P.S. Chae, L. Guan, Effect of Detergents on Galactoside Binding by Melibiose Permeases, Biochemistry. 54 (2015) 5849–5855. doi:10.1021/acs.biochem.5b00660.

[39] C. Nasrallah, K. Rottier, R. Marcellin, V. Compan, J. Font, A. Llebaria, J.-P. Pin, J.-L. Banères, G. Lebon, Direct coupling of detergent purified human mGlu5 receptor to the heterotrimeric G proteins Gq and Gs, Sci. Rep. 8 (2018) 4407. doi:10.1038/s41598-018-22729-4.

[40] T.S. Owen, D. Salom, W. Sun, K. Palczewski, Increasing the Stability of Recombinant Human Green Cone Pigment, Biochemistry. 57 (2018) 1022–1030. doi:10.1021/acs.biochem.7b01118.

[41] C. Perez, S. Gerber, J. Boilevin, M. Bucher, T. Darbre, M. Aebi, J.-L. Reymond, K.P. Locher, Structure and mechanism of an active lipid-linked oligosaccharide flippase, Nature. 524 (2015) 433–

438. doi:10.1038/nature14953.

[42] E.M. Quistgaard, M. Martinez Molledo, C. Löw, Structure determination of a major facilitator peptide transporter: Inward facing PepTSt from Streptococcus thermophilus crystallized in space group P3121, PloS One. 12 (2017) e0173126. doi:10.1371/journal.pone.0173126.

[43] Y. Gao, G. Westfield, J.W. Erickson, R.A. Cerione, G. Skiniotis, S. Ramachandran, Isolation and structure-function characterization of a signaling-active rhodopsin-G protein complex, J. Biol. Chem. 292 (2017) 14280–14289. doi:10.1074/jbc.M117.797100.

[44] K.Y. Chung, T.H. Kim, A. Manglik, R. Alvares, B.K. Kobilka, R.S. Prosser, Role of detergents in conformational exchange of a G protein-coupled receptor, J. Biol. Chem. 287 (2012) 36305–36311. doi:10.1074/jbc.M112.406371.

[45] K.Y. Chung, S.G.F. Rasmussen, T. Liu, S. Li, B.T. DeVree, P.S. Chae, D. Calinski, B.K. Kobilka, V.L. Woods Jr, R.K. Sunahara, Conformational changes in the G protein Gs induced by the β2 adrenergic receptor, Nature. 477 (2011) 611–615. doi:10.1038/nature10488.

[46] G.H. Westfield, S.G.F. Rasmussen, M. Su, S. Dutta, B.T. DeVree, K.Y. Chung, D. Calinski, G. Velez-Ruiz, A.N. Oleskie, E. Pardon, P.S. Chae, T. Liu, S. Li, V.L. Woods Jr, J. Steyaert, B.K. Kobilka, R.K. Sunahara, G. Skiniotis, Structural flexibility of the G alpha s alpha-helical domain in the beta2-adrenoceptor Gs complex, Proc. Natl. Acad. Sci. U. S. A. 108 (2011) 16086–16091. doi:10.1073/pnas.1113645108.

[47] F. Hauer, C. Gerle, N. Fischer, A. Oshima, K. Shinzawa-Itoh, S. Shimada, K. Yokoyama, Y. Fujiyoshi, H. Stark, GraDeR: Membrane Protein Complex Preparation for Single-Particle Cryo-EM, Struct. Lond. Engl. 1993. 23 (2015) 1769–1775. doi:10.1016/j.str.2015.06.029.

[48] T.E. Kraft, R.C. Hresko, P.W. Hruz, Expression, purification, and functional characterization of the insulin-responsive facilitative glucose transporter GLUT4, Protein Sci. Publ. Protein Soc. 24 (2015) 2008–2019. doi:10.1002/pro.2812.

[49] K.H. Cho, M. Husri, A. Amin, K. Gotfryd, H.J. Lee, J. Go, J.W. Kim, C.J. Loland, L. Guan, B. Byrne, P.S. Chae, Maltose neopentyl glycol-3 (MNG-3) analogues for membrane protein study, The Analyst. 140 (2015) 3157–3163. doi:10.1039/c5an00240k.

[50] S.E. Rollauer, M.J. Tarry, J.E. Graham, M. Jääskeläinen, F. Jäger, S. Johnson, M. Krehenbrink, S.-M. Liu, M.J. Lukey, J. Marcoux, M.A. McDowell, F. Rodriguez, P. Roversi, P.J. Stansfeld, C.V. Robinson, M.S.P. Sansom, T. Palmer, M. Högbom, B.C. Berks, S.M. Lea, Structure of the TatC core of the twin-arginine protein transport system, Nature. 492 (2012) 210–214. doi:10.1038/nature11683.

[51] B.H. Thurtle-Schmidt, R.M. Stroud, Structure of Bor1 supports an elevator transport mechanism for SLC4 anion exchangers, Proc. Natl. Acad. Sci. U. S. A. 113 (2016) 10542–10546. doi:10.1073/pnas.1612603113.

[52] J. Guo, W. Zeng, Q. Chen, C. Lee, L. Chen, Y. Yang, C. Cang, D. Ren, Y. Jiang, Structure of the voltage-gated two-pore channel TPC1 from Arabidopsis thaliana, Nature. 531 (2016) 196–201. doi:10.1038/nature16446.

[53] K.W. Huynh, M.R. Cohen, J. Jiang, A. Samanta, D.T. Lodowski, Z.H. Zhou, V.Y. Moiseenkova-Bell, Structure of the full-length TRPV2 channel by cryo-EM, Nat. Commun. 7 (2016) 11130. doi:10.1038/ncomms11130.

[54] A. Oshima, K. Tani, Y. Fujiyoshi, Atomic structure of the innexin-6 gap junction channel determined by cryo-EM, Nat. Commun. 7 (2016) 13681. doi:10.1038/ncomms13681.

[55] S. Dang, S. Feng, J. Tien, C.J. Peters, D. Bulkley, M. Lolicato, J. Zhao, K. Zuberbühler, W. Ye, L. Qi, T. Chen, C.S. Craik, Y.N. Jan, D.L. Minor, Y. Cheng, L.Y. Jan, Cryo-EM structures of the TMEM16A calcium-activated chloride channel, Nature. 552 (2017) 426–429. doi:10.1038/nature25024.

[56] A.D. Ferguson, J. Breed, K. Diederichs, W. Welte, J.W. Coulton, An internal affinity-tag for purification and crystallization of the siderophore receptor FhuA, integral outer membrane protein from Escherichia coli K-12, Protein Sci. 7 (1998) 1636–8.

[57] M. Roth, P. Carpentier, O. Kaïkati, J. Joly, P. Charrault, M. Pirocchi, R. Kahn, E. Fanchon, L. Jacquamet, F. Borel, A. Bertoni, P. Israel-Gouy, J.L. Ferrer, FIP: a highly automated beamline for multiwavelength anomalous diffraction experiments, Acta Crystallogr. D Biol. Crystallogr. 58 (2002) 805–814.

[58] W. Kabsch, XDS, Acta Crystallogr. D Biol. Crystallogr. 66 (2010) 125–132. doi:10.1107/S0907444909047337.

[59] A.J. McCoy, R.W. Grosse-Kunstleve, P.D. Adams, M.D. Winn, L.C. Storoni, R.J. Read, Phaser crystallographic software, J. Appl. Crystallogr. 40 (2007) 658–674. doi:10.1107/S0021889807021206.

[60] P.V. Afonine, R.W. Grosse-Kunstleve, N. Echols, J.J. Headd, N.W. Moriarty, M. Mustyakimov, T.C. Terwilliger, A. Urzhumtsev, P.H. Zwart, P.D. Adams, Towards automated crystallographic structure refinement with phenix.refine, Acta Crystallogr. D Biol. Crystallogr. 68 (2012) 352–367. doi:10.1107/S0907444912001308.

[61] J.J. Headd, N. Echols, P.V. Afonine, R.W. Grosse-Kunstleve, V.B. Chen, N.W. Moriarty, D.C. Richardson, J.S. Richardson, P.D. Adams, Use of knowledge-based restraints in phenix.refine to improve macromolecular refinement at low resolution, Acta Crystallogr. D Biol. Crystallogr. 68 (2012) 381–390. doi:10.1107/S0907444911047834.

[62] C. Hajjar, M.V. Cherrier, G. Dias Mirandela, I. Petit-Hartlein, M.J. Stasia, J.C. Fontecilla-Camps, F. Fieschi, J. Dupuy, The NOX Family of Proteins Is Also Present in Bacteria, MBio. 8 (2017). doi:10.1128/mBio.01487-17.

[63] E. Steinfels, C. Orelle, O. Dalmas, F. Penin, B. Miroux, A. Di Pietro, J.-M. Jault, Highly efficient over-production in E. coli of YvcC, a multidrug-like ATP-binding cassette transporter from Bacillus subtilis, Biochim. Biophys. Acta. 1565 (2002) 1–5.

[64] C. Orelle, O. Dalmas, P. Gros, A. Di Pietro, J.-M. Jault, The conserved glutamate residue adjacent to the Walker-B motif is the catalytic base for ATP hydrolysis in the ATP-binding cassette transporter BmrA, J. Biol. Chem. 278 (2003) 47002–47008. doi:10.1074/jbc.M308268200.

[65] A. Salvay, C. Ebel, Analytical Ultracentrifuge for the Characterization of Detergent in Solution, in: Prog. Colloid Polym. Sci., 2006: pp. 74–82. doi:10.1007/2882_006.

[66] P. Schuck, Size-distribution analysis of macromolecules by sedimentation velocity ultracentrifugation and lamm equation modeling, Biophys. J. 78 (2000) 1606–1619. doi:10.1016/S0006-3495(00)76713-0.

[67] H. Zhao, R. Ghirlando, C. Alfonso, F. Arisaka, I. Attali, D.L. Bain, M.M. Bakhtina, D.F. Becker, G.J. Bedwell, A. Bekdemir, T.M.D. Besong, C. Birck, C.A. Brautigam, W. Brennerman, O. Byron, A. Bzowska, J.B. Chaires, C.T. Chaton, H. Cölfen, K.D. Connaghan, K.A. Crowley, U. Curth, T. Daviter, W.L. Dean, A.I. Díez, C. Ebel, D.M. Eckert, L.E. Eisele, E. Eisenstein, P. England, C. Escalante, J.A. Fagan, R. Fairman, R.M. Finn, W. Fischle, J.G. de la Torre, J. Gor, H. Gustafsson, D. Hall, S.E. Harding, J.G.H. Cifre, A.B. Herr, E.E. Howell, R.S. Isaac, S.-C. Jao, D. Jose, S.-J. Kim, B.

Kokona, J.A. Kornblatt, D. Kosek, E. Krayukhina, D. Krzizike, E.A. Kusznir, H. Kwon, A. Larson, T.M. Laue, A. Le Roy, A.P. Leech, H. Lilie, K. Luger, J.R. Luque-Ortega, J. Ma, C.A. May, E.L. Maynard, A. Modrak-Wojcik, Y.-F. Mok, N. Mücke, L. Nagel-Steger, G.J. Narlikar, M. Noda, A. Nourse, T. Obsil, C.K. Park, J.-K. Park, P.D. Pawelek, E.E. Perdue, S.J. Perkins, M.A. Perugini, C.L. Peterson, M.G. Peverelli, G. Piszczek, G. Prag, P.E. Prevelige, B.D.E. Raynal, L. Rezabkova, K. Richter, A.E. Ringel, R. Rosenberg, A.J. Rowe, A.C. Rufer, D.J. Scott, J.G. Seravalli, A.S. Solovyova, R. Song, D. Staunton, C. Stoddard, K. Stott, H.M. Strauss, W.W. Streicher, J.P. Sumida, S.G. Swygert, R.H. Szczepanowski, I. Tessmer, R.T. Toth, A. Tripathy, S. Uchiyama, S.F.W. Uebel, S. Unzai, A.V. Gruber, P.H. von Hippel, C. Wandrey, S.-H. Wang, S.E. Weitzel, B. Wielgus-Kutrowska, C. Wolberger, M. Wolff, E. Wright, Y.-S. Wu, J.M. Wubben, P. Schuck, A multilaboratory comparison of calibration accuracy and the performance of external references in analytical ultracentrifugation, PloS One. 10 (2015) e0126420. doi:10.1371/journal.pone.0126420.

[68] C.A. Brautigam, Calculations and Publication-Quality Illustrations for Analytical Ultracentrifugation Data, Methods Enzymol. 562 (2015) 109–133. doi:10.1016/bs.mie.2015.05.001.

[69] A. Le Roy, H. Nury, B. Wiseman, J. Sarwan, J.-M. Jault, C. Ebel, Sedimentation velocity analytical ultracentrifugation in hydrogenated and deuterated solvents for the characterization of membrane proteins, Methods Mol. Biol. Clifton NJ. 1033 (2013) 219–251. doi:10.1007/978-1-62703-487-6_15.

[70] A. Le Roy, K. Wang, B. Schaack, P. Schuck, C. Breyton, C. Ebel, AUC and Small-Angle Scattering for Membrane Proteins, Methods Enzymol. 562 (2015) 257–286. doi:10.1016/bs.mie.2015.06.010.

[71] A.G. Salvay, M. Santamaria, M. le Maire, C. Ebel, Analytical ultracentrifugation sedimentation velocity for the characterization of detergent-solubilized membrane proteins Ca++-ATPase and ExbB, J. Biol. Phys. 33 (2007) 399–419. doi:10.1007/s10867-008-9058-3.

[72] P. Pernot, A. Round, R. Barrett, A. De Maria Antolinos, A. Gobbo, E. Gordon, J. Huet, J. Kieffer, M. Lentini, M. Mattenet, C. Morawe, C. Mueller-Dieckmann, S. Ohlsson, W. Schmid, J. Surr, P. Theveneau, L. Zerrad, S. McSweeney, Upgraded ESRF BM29 beamline for SAXS on macromolecules in solution, J. Synchrotron Radiat. 20 (2013) 660–664. doi:10.1107/S0909049513010431.

[73] M.V. Petoukhov, D. Franke, A.V. Shkumatov, G. Tria, A.G. Kikhney, M. Gajda, C. Gorba, H.D.T. Mertens, P.V. Konarev, D.I. Svergun, New developments in the ATSAS program package for small-angle scattering data analysis, J. Appl. Crystallogr. 45 (2012) 342–350. doi:10.1107/S0021889812007662.

[74] C. Ebel, C. Breyton, A. Martel, Examining membrane proteins by neutron scattering, in: Biophys. Membr. Proteins Methods Protoc., Springer, Vincent Postis and Adrian Goldmann, 2018.

[75] S.R. Kline, Reduction and analysis of SANS and USANS data using IGOR Pro, J. Appl. Crystallogr. 39 (2006) 895–900. doi:10.1107/S0021889806035059.

[76] M. Doucet, J.H. Cho, G. Alina, J. Bakker, W. Bouwman, P. Butler, K. Campbell, M. Gonzales, R. Heenan, A. Jackson, P. Juhas, S. King, P. Kienzle, J. Krzywon, A. Markvardsen, T. Nielsen, L. O'Driscoll, W. Potrzebowski, R. Ferraz Leal, T. Richter, P. Rozycko, T. Snow, A. Washington, SasView version 4.2, Zenodo, 2018. doi:10.5281/zenodo.1412041.

[77] C. Breyton, F. Gabel, M. Lethier, A. Flayhan, G. Durand, J.-M. Jault, C. Juillan-Binard, L. Imbert, M. Moulin, S. Ravaud, M. Härtlein, C. Ebel, Small angle neutron scattering for the study of solubilised membrane proteins, Eur. Phys. J. E Soft Matter. 36 (2013) 9889. doi:10.1140/epje/i2013-13071-6.

[78] A. Flayhan, F. Wien, M. Paternostre, P. Boulanger, C. Breyton, New insights into pb5, the receptor binding protein of bacteriophage T5, and its interaction with its Escherichia coli receptor FhuA, Biochimie. 94 (2012) 1982–1989. doi:10.1016/j.biochi.2012.05.021.

[79] C. Breyton, A. Flayhan, F. Gabel, M. Lethier, G. Durand, P. Boulanger, M. Chami, C. Ebel, Assessing the Conformational Changes of pb5, the Receptor-binding Protein of Phage T5, upon Binding to Its Escherichia coli Receptor FhuA, J. Biol. Chem. 288 (2013) 30763–30772. doi:10.1074/jbc.M113.501536.

[80] A.D. Ferguson, E. Hofmann, J.W. Coulton, K. Diederichs, W. Welte, Siderophore-mediated iron transport: crystal structure of FhuA with bound lipopolysaccharide, Science. 282 (1998) 2215–20.

[81] M. Bonhivers, M. Desmadril, G.S. Moeck, P. Boulanger, A. Colomer-Pallas, L. Letellier, Stability studies of FhuA, a two-domain outer membrane protein from Escherichia coli, Biochemistry. 40 (2001) 2606–13.

[82] P. Boulanger, M. le Maire, M. Bonhivers, S. Dubois, M. Desmadril, L. Letellier, Purification and structural and functional characterization of FhuA, a transporter of the Escherichia coli outer membrane, Biochemistry. 35 (1996) 14216–14224. doi:10.1021/bi9608673.

[83] D. Durand, C. Vivès, D. Cannella, J. Pérez, E. Pebay-Peyroula, P. Vachette, F. Fieschi, NADPH oxidase activator p67(phox) behaves in solution as a multidomain protein with semi-flexible linkers, J. Struct. Biol. 169 (2010) 45–53. doi:10.1016/j.jsb.2009.08.009.

[84] J. Marcoux, P. Man, I. Petit-Haertlein, C. Vivès, E. Forest, F. Fieschi, p47phox molecular activation for assembly of the neutrophil NADPH oxidase complex, J. Biol. Chem. 285 (2010) 28980–28990. doi:10.1074/jbc.M110.139824.

[85] F. Magnani, S. Nenci, E. Millana Fananas, M. Ceccon, E. Romero, M.W. Fraaije, A. Mattevi, Crystal structures and atomic model of NADPH oxidase, Proc. Natl. Acad. Sci. U. S. A. 114 (2017) 6764–6769. doi:10.1073/pnas.1702293114.

[86] E. Steinfels, C. Orelle, J.-R. Fantino, O. Dalmas, J.-L. Rigaud, F. Denizot, A. Di Pietro, J.-M. Jault, Characterization of YvcC (BmrA), a multidrug ABC transporter constitutively expressed in Bacillus subtilis, Biochemistry. 43 (2004) 7491–7502. doi:10.1021/bi0362018.

[87] A. Ward, C.L. Reyes, J. Yu, C.B. Roth, G. Chang, Flexibility in the ABC transporter MsbA: Alternating access with a twist, Proc. Natl. Acad. Sci. U. S. A. 104 (2007) 19005–19010. doi:10.1073/pnas.0709388104.

[88] M.S. Jin, M.L. Oldham, Q. Zhang, J. Chen, Crystal structure of the multidrug transporter P-glycoprotein from Caenorhabditis elegans, Nature. 490 (2012) 566–569. doi:10.1038/nature11448.

[89] S. Ravaud, M.-A. Do Cao, M. Jidenko, C. Ebel, M. Le Maire, J.-M. Jault, A. Di Pietro, R. Haser, N. Aghajari, The ABC transporter BmrA from Bacillus subtilis is a functional dimer when in a detergent-solubilized state, Biochem. J. 395 (2006) 345–53.

[90] O. Dalmas, M.-A. Do Cao, M.R. Lugo, F.J. Sharom, A. Di Pietro, J.-M. Jault, Time-resolved fluorescence resonance energy transfer shows that the bacterial multidrug ABC half-transporter BmrA functions as a homodimer, Biochemistry. 44 (2005) 4312–4321. doi:10.1021/bi0482809.

[91] C. Orelle, F. Gubellini, A. Durand, S. Marco, D. Lévy, P. Gros, A. Di Pietro, J.-M. Jault, Conformational change induced by ATP binding in the multidrug ATP-binding cassette transporter BmrA, Biochemistry. 47 (2008) 2404–2412. doi:10.1021/bi702303s.

[92] M.-A. Do Cao, S. Crouzy, M. Kim, M. Becchi, D.S. Cafiso, A. Di Pietro, J.-M. Jault, Probing the conformation of the resting state of a bacterial multidrug ABC transporter, BmrA, by a site-

directed spin labeling approach, Protein Sci. Publ. Protein Soc. 18 (2009) 1507–1520. doi:10.1002/pro.141.

[93] S. Mehmood, C. Domene, E. Forest, J.-M. Jault, Dynamics of a bacterial multidrug ABC transporter in the inward- and outward-facing conformations, Proc. Natl. Acad. Sci. U. S. A. 109 (2012) 10832–10836. doi:10.1073/pnas.1204067109.

[94] P.F. Fribourg, M. Chami, C.O.S. Sorzano, F. Gubellini, R. Marabini, S. Marco, J.-M. Jault, D. Lévy, 3D cryo-electron reconstruction of BmrA, a bacterial multidrug ABC transporter in an inward-facing conformation and in a lipidic environment, J. Mol. Biol. 426 (2014) 2059–2069. doi:10.1016/j.jmb.2014.03.002.

[95] B. Wiseman, A. Kilburg, V. Chaptal, G.C. Reyes-Mejia, J. Sarwan, P. Falson, J.-M. Jault, Stubborn contaminants: influence of detergents on the purity of the multidrug ABC transporter BmrA, PloS One. 9 (2014) e114864. doi:10.1371/journal.pone.0114864.

[96] J. Lipfert, L. Columbus, V.B. Chu, S.A. Lesley, S. Doniach, Size and shape of detergent micelles determined by small-angle X-ray scattering, J. Phys. Chem. B. 111 (2007) 12427–12438. doi:10.1021/jp073016l.

[97] R.C. Oliver, S.V. Pingali, V.S. Urban, Designing Mixed Detergent Micelles for Uniform Neutron Contrast, J. Phys. Chem. Lett. 8 (2017) 5041–5046. doi:10.1021/acs.jpclett.7b02149.

[98] J.N. Israelachvili, D.J. Mitchell, B.W. Barry W. Ninham, Theory of self-assembly of lipid bilayers and vesicles, Biochim Biophys Acta - Biomembr. 470 (1977) 185–201.

[99] J.N. Israelachvili, Intermolecular and Surface Forces - 3rd Edition, London: Academic Press, 1992. https://www.elsevier.com/books/intermolecular-and-surface-forces/israelachvili/978-0-12-391927-4 (accessed July 24, 2018).

[100] C. Breyton, F. Gabel, M. Abla, Y. Pierre, F. Lebaupain, G. Durand, J.-L. Popot, C. Ebel, B. Pucci, Micellar and biochemical properties of (hemi)fluorinated surfactants are controlled by the size of the polar head, Biophys. J. 97 (2009) 1077–1086. doi:10.1016/j.bpj.2009.05.053.

[101] E. Boncoeur, C. Durmort, B. Bernay, C. Ebel, A.M. Di Guilmi, J. Croizé, T. Vernet, J.-M. Jault, PatA and PatB form a functional heterodimeric ABC multidrug efflux transporter responsible for the resistance of Streptococcus pneumoniae to fluoroquinolones, Biochemistry. 51 (2012) 7755–7765. doi:10.1021/bi300762p.

[102] E. Pebay-Peyroula, G. Rummel, J.P. Rosenbusch, E. Landau, X-ray structure of bacteriorhodopsin at 2.5 Å from microcrystals grown in lipidic cubic phases, Science. 277 (1997) 1676–1881.